Please contact Claire Zarakas (czarakas@uw.edu) regarding this manuscript's content

Different model assumptions about plant hydraulics and photosynthetic temperature acclimation yield diverging implications for tropical forest resilience

Claire M. Zarakas[1], Abigail L. S. Swann[1,2], Charles Koven[3], Marielle N. Smith[4,5], and Tyeen C. Taylor[6]

[1]Department of Atmospheric Sciences, University of Washington, Seattle, WA, USA

[2]Department of Biology, University of Washington, Seattle, WA, USA

[3]Lawrence Berkeley National Laboratory, Berkeley, CA, USA

[4]Department of Forestry, Michigan State University, East Lansing, MI, USA

[5]School of Environmental and Natural Sciences, College of Environmental Sciences and Engineering, Bangor University, Bangor, UK

[6]University of Michigan, Department of Civil and Environmental Engineering, Ann Arbor, Michigan, USA

Corresponding author: Claire M. Zarakas, `czarakas@uw.edu`

Abstract

Tropical forest photosynthesis can decline at high temperatures due to (1) biochemical responses to increasing temperature and (2) stomatal responses to increasing vapor pressure deficit (VPD), which is associated with increasing temperature. It is challenging to disentangle the influence of these two mechanisms on photosynthesis in observations, because temperature and VPD are tightly correlated in tropical forests. Nonetheless, quantifying the relative strength of these two mechanisms is essential for understanding how tropical gross primary productivity (GPP) will respond to climate change, because increasing atmospheric CO_2 concentration may partially offset VPD-driven stomatal responses, but is not expected to mitigate the effects of temperature-driven biochemical responses. We used two terrestrial biosphere models to quantify how physiological process assumptions (photosynthetic temperature acclimation and plant hydraulic stress) and functional traits (e.g. maximum xylem conductivity) influence the relative strength of modeled temperature vs. VPD effects on light-saturated GPP at an Amazonian forest site, a seasonally dry tropical forest site, and an experimental tropical forest mesocosm. By simulating idealized climate change scenarios, we quantified the divergence in GPP predictions under model configurations with stronger VPD effects compared to stronger direct temperature effects. Assumptions consistent with stronger direct temperature effects resulted in larger GPP declines under warming, while assumptions consistent with stronger VPD effects resulted in more resilient GPP under warming. Our findings underscore the importance of quantifying the role of direct temperature and indirect VPD effects for projecting the resilience of tropical forests in the future, and demonstrate that the relative strength of temperature vs. VPD effects in models is highly sensitive to plant functional parameters and structural assumptions about photosynthetic temperature acclimation and plant hydraulics.

Keywords:

- Vapor pressure deficit
- Temperature
- Photosynthesis
- Stomatal conductance
- Temperature sensitivity
- Acclimation

1 Introduction

Predicting how projected temperature increases will impact the tropical forest carbon sink requires understanding how tropical forest photosynthesis responds to increasing temperature. Photosynthesis, like most biological processes, is temperature dependent, with photosynthesis-temperature response curves exhibiting a temperature optimum above which photosynthetic rates decline. Some studies suggest that tropical forests may already exist near their current optimum temperature (Doughty & Goulden, 2008; Mau et al., 2018; Huang et al., 2019; Duffy et al., 2021; Doughty et al., 2023), but this is a subject of ongoing debate (Lloyd & Farquhar, 2008; Tan et al., 2017). It remains unclear what processes drive ecosystem-level photosynthetic declines beyond forests' apparent temperature optima, and it is likewise unclear how photosynthetic rates will respond to further increases in air temperature due to climate change.

It is challenging to quantify tropical forests' direct photosynthetic response to temperature from observations because temperature is highly correlated with vapor pressure deficit (VPD), which also directly impacts photosynthesis. Observed photosynthetic declines associated with temperatures beyond a forest's thermal optimum can therefore result from two distinct mechanisms: (1) direct temperature effects on photosynthesis and (2) VPD effects on photosynthesis. VPD effects can also be considered indirect temperature effects because temperature directly controls the saturation vapor pressure of air, so increasing temperature increases VPD even if the water content of the air, or more conservatively the relative humidity, remains constant.

Direct temperature effects result from biochemical responses to high temperatures. Temperature controls enzymes' activity rates, and biochemical responses to increasing temperature beyond a plant's thermal optimum can lead to reversible downregulation of photosynthesis. Very high temperatures (e.g. leaf temperature greater than 40°C) can cause permanent damage to photosynthetic machinery, leading to longer-term suppression of photosynthetic capacity (Grossiord et al., 2020). Under sustained temperature increases, observations indicate that plants can acclimate to higher temperatures by shifting their photosynthetic thermal optima closer to ambient temperatures (Kattge & Knorr, 2007; Kumarathunge et al., 2019).

Meanwhile, VPD effects are due to reversible stomatal responses to atmospheric demand for water. Leaves' stomata close with increasing VPD in order to minimize wa-

ter loss, and this stomatal closure reduces leaf-level photosynthesis. Increasing VPD reduces stomatal conductance even under well-watered conditions (Medlyn et al., 2011), and leaf water declines driven by plant hydraulic limitations on supplying water to leaves can further amplify VPD-driven stomatal conductance declines (Grossiord et al., 2020).

While it is challenging to disentangle these two mechanisms, it is nonetheless essential to do so in order to project how tropical gross primary productivity (GPP) will respond to climate change. Future relationships between temperature and VPD are expected to deviate from present day temperature-VPD relationships because global warming tends to decrease relative humidity over land, reflecting that increases in land evapotranspiration and moisture import from the ocean are not expected to keep up with increasing temperature under global warming (Byrne & O'Gorman, 2018). Empirical estimates of GPP sensitivity to temperature that implicitly include VPD effects (or vice versa) only work in a stationary temperature-VPD regime, so they may not hold in a warmer climate. Furthermore, increasing atmospheric CO_2 concentrations may partially offset VPD-driven stomatal responses (Lloyd & Farquhar, 2008; Dusenge et al., 2019), but are not expected to mitigate the effects of temperature-driven biochemical responses.

The challenge of disentangling temperature and VPD effects has led to substantial discussion of the extent to which VPD vs. direct temperature effects are driving observed photosynthetic declines with temperature in tropical forests, with some evidence for both effects. Many recent observational studies support the hypothesis that, in the present day, VPD effects are stronger than direct temperature effects, based on leaf gas exchange measurements (Vargas-G & Cordero, 2013; Slot & Winter, 2016; Slot et al., 2016; Santos et al., 2018), analysis of ecosystem-level observations (Wu et al., 2017; Santos et al., 2018; Fu et al., 2018), and experimental decoupling of temperature and VPD (Smith et al., 2020). However, some analysis of leaf-level observations suggest that direct temperature effects may be substantial for some tropical tree species (Slot and Winter 2017a,b; Doughty et al. 2023).

Terrestrial biosphere models differ in the strength of temperature and VPD effects under present day and future conditions. Rowland et al. (2015) compared five land system models under present day conditions, and found that modeled VPD effects are stronger than direct temperature effects in all models, but that the magnitude of overall (temperature + VPD effects) varies substantially across models. Galbraith et al. (2010) found

that in a high-emissions scenario, Amazonian total vegetation carbon decreased, but that the extent to which this was due to temperature vs. VPD effects varied across three models - in two models, direct temperature effects dominated, and in one model temperature and VPD effects contributed approximately equally to vegetation carbon declines. It is challenging to determine exactly what drives differences in the strength of temperature and VPD effects between models, because in modern land models temperature and VPD effects on GPP are emergent properties that result from multiple leaf-, plant-, and ecosystem-level processes. Temperature and VPD effects can vary between models due to different assumptions about the temperature responses of photosynthetic rates (Galbraith et al., 2010; Rowland et al., 2015), stomatal conductance, plant hydraulics, plant functional traits, and other plant and soil processes which indirectly control photosynthesis and stomatal conductance.

In this study, we systematically quantified how different model assumptions control the strength of temperature and VPD effects (as measured via the GPP responses of tropical forests) in models on hourly timescales, and present a framework for comparing model hypotheses with ecosystem-level observational constraints. We focused on the impacts of plant hydraulics and photosynthetic temperature acclimation because previous work has shown that they influence plants' responses to temperature and VPD (Lombardozzi et al., 2015; Kennedy et al., 2019), but most land surface models used to assess global carbon cycle feedbacks do not include either process (Table S1). In our analysis, we distinguished between structural assumptions (what equations are used to represent plant processes, e.g. the equations that govern water transport along the soil-plant-atmosphere continuum) and parameter assumptions (how those equations are parameterized, e.g. the value for maximum xylem conductivity). We asked the following questions: (1) How do photosynthetic temperature acclimation and plant hydraulics influence the modeled strength of temperature vs. VPD effects on GPP? (2) How do plant functional traits control apparent GPP responses to temperature? (3) Which structural and parameter assumptions are consistent with observed variations in the apparent GPP sensitivity to temperature across three different tropical forest sites? and (4) How do different assumptions about the relative strength of temperature vs. VPD effects influence projected GPP responses to warming?

2 Methods

2.1 Site descriptions

We analyzed three tropical forest sites which span distinct temperature-VPD regimes (Figure S1): the Biosphere 2 experimental tropical forest (B2), the kilometer 67 Amazonian evergreen forest eddy covariance site (K67), and the Tesopaco Mexican tropical deciduous forest eddy covariance site (MX-Tes). All sites regularly exceed 30°C, but the typical VPD at 30°C differs between the sites: 0.75 kPa (B2), 1.49 kPa (K67), and 2.75 kPa (MX-Tes).

K67 is a tropical evergreen forest located in the Tapajós National Forest near Santarém, Pará, Brazil, and the site is described in more detail in Hutyra et al. (2007) and Restrepo-Coupe et al. (2013). Eddy covariance data for this site was collected by the Large-scale Biosphere-Atmosphere Experiment in Amazonia (LBA). K67 experiences an annual mean temperature of 26°C, annual mean relative humidity of 84.6%, and 1,993 mm mean annual rainfall. Temperatures can reach up to 33°C on hourly timescales.

MX-Tes is a tropical dry deciduous forest in Sonora, Mexico (Perez-Ruiz et al., 2010). The mean annual temperature at MX-Tes is 24°C, mean relative humidity is 48%, and hourly temperatures can reach up to 42°C. The site receives 712 mm mean annual rainfall, which primarily falls during the July-September wet season, and most trees lose their leaves during the dry season. We only analyzed data from Tesopaco during the growing season, which we defined as July to September based on leaf area index observations (Smith et al., 2020).

B2 is an experimental evergreen tropical forest biome within the Biosphere 2 Earth science facility in Arizona, USA. The mean annual temperature at B2 is 27.2°C, and hourly temperatures can reach up to 49°C. The annual mean rainfall is 1,300 mm and mean relative humidity is 82%. B2 differs from natural tropical forests in several ways. Firstly, B2 maintains high humidity levels even at temperatures greater than 30°C, which means the VPD associated with a given temperature is typically lower than it would be in a natural tropical temperature-VPD regime (Smith et al., 2020, Figure S1). Additionally, the seasonality of temperature and VPD is stronger in B2, and there is no rainfall seasonality. B2 also experiences lower solar radiation and higher CO_2 concentrations than

natural forest sites. Differences between B2 and natural tropical forests are discussed in more depth in Smith et al. (2020), Rosolem et al. (2010), and Arain et al. (2000).

2.2 Model descriptions

We ran simulations using two different models: the Functionally Assembled Terrestrial Ecosystem Simulator (FATES; Koven et al., 2020) and the Community Land Model version 5 (CLM5; Lawrence et al., 2019). We ran single-site simulations of K67, B2, and MX-Tes from 2002-2011, 1998-2003, and 2004-2009, respectively, with simulations forced with gap-filled historical meteorological data. For each model, we ran four different model configurations where we turned on and off photosynthetic temperature acclimation and plant hydraulics.

2.2.1 FATES model

FATES is a size- and age-structured vegetation demographic model. We used the static stand structure configuration of the model, a reduced complexity mode in which a site's stand structure and leaf area are held constant over time, initialized from forest inventory data. This configuration allows us to look at the direct response of ecosystem function to parameter and structural perturbation, in the absence of internal feedbacks due to the effects of growth and mortality on ecosystem function. The default FATES model configuration represents stomatal conductance using the Ball-Berry model (Ball et al., 1987).

The default FATES configuration ($\text{FATES}_{\text{NoAcclimNoHydro}}$) does not include either photosynthetic temperature acclimation or plant hydraulics. In a modified version of FATES, $\text{FATES}_{\text{HydroOnly}}$, we turned on the plant hydraulics module (Christoffersen et al., 2016; C. Xu et al., 2023), which dynamically calculates water transport along the soil-plant-atmosphere continuum and determines vegetation water stress as a function of leaf water potential. In another modified FATES version, $\text{FATES}_{\text{AcclimOnly}}$, we implemented the photosynthetic temperature acclimation scheme developed by Kumarathunge et al. (2019), which allows plants to change the temperature dependence of photosynthetic rates based on growth temperature. In $\text{FATES}_{\text{AcclimAndHydro}}$ we turned on both plant hydraulics and photosynthetic temperature acclimation.

	Variable	ΔH_a (J/mol)	ΔH_d (J/mol)	ΔS (J/mol/K)
Default FATES	J_{max}	43,540	152,040	495
	V_{cmax}	65,330	149,250	485
Modified Kumarathunge Scheme	J_{max}	40,710	200,000	658.77 - $0.84T_{growth}$
	V_{cmax}	42.6 + $1{,}140T_{growth}$	200,000	645.13 - $0.38T_{growth}$

Table 1. Temperature dependence parameters for photosynthesis.

In the default FATES configuration ($\text{FATES}_{\text{NoAcclimNoHydro}}$), J_{max} and V_{cmax} change with leaf temperature (T_v) according the peaked Arrhenius function (Equation 1):

$$f(T_v) = exp\left(\frac{\Delta H_a}{298.15R}\left(1 - \frac{298.15}{T_v}\right)\right)\left(\frac{1 + exp(\frac{298.15\Delta S - \Delta H_d}{298.15R})}{1 + exp(\frac{T_v\Delta S - \Delta H_d}{T_v R})}\right) \quad (1)$$

where R is the universal gas constant, ΔH_a is the activation energy term (J/mol), ΔH_d is the deactivation energy term (J/mol), and ΔS is the entropy term (J/K/mol). In default FATES, the temperature dependence parameters for C3 photosynthesis (ΔH_a, ΔH_d, and ΔS) are constant for all C3 plants (Table 1). In the observationally derived Kumarathunge et al. (2019) temperature acclimation scheme, these temperature dependence parameters can acclimate to adjust to plants' growth temperature (T_{growth}) and home temperature (T_{home}), where T_{growth} is defined as the average temperature over the previous 30 days (limited to the range 3-37°C), and T_{home} is defined as the long-term mean maximum temperature of the warmest month of the year (Table 1).

The Kumarathunge temperature acclimation scheme also allows the ratio of J_{max} to V_{cmax} to change based on T_{growth} and T_{home} (Equation 2).

$$JV_r = \frac{J_{max}}{V_{cmax}} = 2.56 - 0.0375T_{home} - 0.0202(T_{growth} - T_{home}) \quad (2)$$

Our temperature acclimation scheme deviates slightly from the original Kumarthunge scheme, because we include only temperature acclimation, and not temperature adaptation effects (which allows plants to adjust their J_{max} temperature dependence curve based on the temperature at the species' seed source, T_{home}). We chose to ignore tem-

perature adaptation effects because in an Earth system modeling context it is challenging to determine a plant functional type's climate of origin in a way that is scalable to the whole globe in both past, present, and future climates, and because Kumarathunge et al. (2019) found that acclimation was a stronger driver of variation in plants' photosynthetic thermal optima than adaptation was. Our modified Kumarathunge scheme (Table 1) is identical to the full Kumarathunge et al. (2019) scheme under the condition where $T_{home} = T_{growth}$.

2.2.2 CLM5 model

We used the satellite phenology configuration of CLM5, which is a reduced complexity mode of the model that prescribes leaf area and vegetation height. As with the FATES configuration, this CLM5 configuration allowed us to isolate direct responses without confounding feedbacks due to changes in leaf area. The default version of CLM5 ($\text{CLM5}_{\text{AcclimAndHydro}}$) includes both plant hydraulics (Kennedy et al., 2019) and the Kattge & Knorr (2007) photosynthetic temperature acclimation scheme (Lombardozzi et al., 2015), and represents stomatal conductance using the Medlyn et al. (2011) model. In addition to the default CLM5 model, we ran three additional model configurations where we turned on and off photosynthetic temperature acclimation and plant hydraulics: $\text{CLM5}_{\text{AcclimOnly}}$, in which we turned off the plant hydraulics module; $\text{CLM5}_{\text{HydroOnly}}$, in which we reverted to the photosynthetic temperature response functions from an older version of CLM (documented in Lombardozzi et al., 2015); and $\text{CLM5}_{\text{NoAcclimNoHydro}}$, in which we turned off both plant hydraulics and photosynthetic temperature acclimation.

2.3 Observational data (environmental driver data, forest structure data, and flux calculations)

We used gap-filled meteorological data and net ecosystem exchange (NEE) data from the FLUXNET2015 dataset (Pastorello et al., 2020) for K67, from Rafael Rosolem (Rosolem et al., 2010; Smith et al., 2020) for B2, and from the AmeriFlux FLUXNET data product for MX-Tes (Yepez & Garatuza, 2021). We calculated GPP by assuming that daily ecosystem respiration rates are equal to night-time NEE following the methodology in Smith et al. (2020).

For CLM5 simulations, we prescribed leaf area and vegetation height based on observations in the literature. At K67 we set leaf area to 6 m^2/m^2 (based on Restrepo-Coupe et al., 2017), at Biosphere 2 we held leaf area constant at 5 m^2/m^2 (based on Rosolem et al., 2010), and and at MX-Tes we prescribed a seasonally varying leaf area index which ranged from 0.3 to 4.1 m^2/m^2 throughout the year, based on the average monthly leaf area index in Smith et al. (2020). We set vegetation height to 33.2 m for K67 (based on the observationally-derived gridded CLM input dataset at that location), 11.5 m for B2 (from B2 forest inventory data) and 14 m for MX-Tes (Sanchez-Mejia et al., 2021).

For FATES simulations, we prescribed the forest structure (tree diameter distribution) to match forest inventory data, and held this forest structure constant over time. We used 2012 forest inventory data for K67, 2000 forest inventory for B2, and 2009 forest inventory data for MX-Tes (Sanchez-Mejia et al., 2021). For B2, we modified FATES' default allometric scaling relationships to achieve the observed distribution of tree heights, which was necessary because B2 trees are shorter for a given stem diameter than trees at natural tropical forests (Rascher et al., 2004; Smith et al., 2020).

Our analysis focused on GPP under high light conditions, and site-specific light saturation thresholds were estimated from observed relationships between downward shortwave radiation and NEE. We used light saturation thresholds of 600 W/m^2 for K67, 300 W/m^2 for MX-Tes, and 200 W/m^2 for B2. We refer to GPP above these light thresholds as light-saturated GPP.

2.4 Synthetic meteorology method for calculating light-saturated GPP responses to temperature and VPD

We calculate light-saturated GPP temperature response curves by binning light-saturated GPP by air temperature in 1°C bins. We refer to the modeled *apparent* GPP temperature response as the binned response curve for actual GPP associated with a given temperature in observations, and we refer to the GPP *direct* temperature response as the binned response curve only due to direct temperature effects, which we quantify using FATES and CLM simulations with synthetic meteorological forcings.

We quantified the extent to which the apparent modeled light-saturated GPP responses to temperature are due to direct temperature effects or VPD effects by running model simulations with synthetic meteorological forcings. We used an "everything but"

approach to quantify the effect of each meteorological driver. For example, the direct effect of temperature on modeled GPP is calculated as the difference between modeled historical GPP (in which the model is forced with the observed historical meteorology) and modeled GPP under a synthetic meteorology where temperature is held constant at 25°C and all other meteorological quantities match the observed historical meteorology. Using this approach, we disentangled the individual contributions of (1) direct temperature effects, (2) VPD effects, (3) synergistic VPD-temperature effects, and (4) all other meteorological effects, including solar radiation and precipitation (Table S2). The sum of these four terms equals the net effect, and the net effect is equivalent to the apparent GPP response in model simulations forced with the observed site meteorology (Text S1). We additionally quantified the effect of soil moisture by running synthetic meteorology simulations where rainfall is held constant throughout the year at 0.005 mm/s, which constantly saturates the soil and relieves any soil moisture stress.

2.5 Perturbed parameter ensemble

We quantified how plant functional traits relating to photosynthesis, stomatal conductance, and plant hydraulics modify the strength of direct and indirect temperature effects by running a small perturbed parameter ensemble in $\text{FATES}_{\text{AcclimAndHydro}}$, where we perturbed plant functional trait parameters one at a time to low-end, median, and high-end values based on the existing literature (Table S3). We ran twelve parameter perturbation simulations for four FATES parameters. We quantified the modeled strength of direct and indirect temperature effects for each ensemble member using the same synthetic meteorology method described above.

2.6 Idealized future climate treatments

We quantified how K67 responds to warming in different model configurations by applying five idealized climate treatments: (1) temperature increase, (2) temperature and VPD increase (under constant relative humidity), (3) temperature increase and relative humidity decrease, (4) VPD increase, (5) relative humidity decrease (Figure S7). We used this factorial idealized climate treatment design in order to disentangle the extent to which GPP changes under warming are due to direct biochemical effects from increasing temperature vs. stomatal effects due to VPD increases, and we assess the impact of constant vs. decreasing relative humidity to represent different expectations about future climate

as described further below. In the temperature increase treatment (1), temperature in the historical meteorological forcing dataset is uniformly increased by 3°C at all points in time, but VPD is held constant at historical levels, and thus relative humidity increases. In the temperature and VPD treatment (2), both temperature and VPD increase to reflect a 3°C warming and constant relative humidity. In the temperature increase and relative humidity decrease (3), temperature increases by 3°C and relative humidity decreases by 6%. This idealized relative humidity decrease is consistent with CMIP6 model projections of Amazon climate change - multi-model mean relative humidity decreases by about 4-7% by midcentury and 4-13% by the end of the century, depending on the scenario (Li et al., 2023). In the VPD increase treatment (4), VPD is increased to reflect the VPD change that would occur under 3°C warming and constant relative humidity, but temperature is held constant at historical levels. In the relative humidity decrease (5), VPD is increased to reflect the VPD change that would occur under 3°C warming and -6% decrease in relative humidity, but temperature is held constant at historical levels. We additionally ran two of these climate treatments (1 and 3 above) under elevated CO_2 concentrations of 560 ppm. We selected this CO_2 concentration because it is two times the preindustrial CO_2 concentrations - in medium to high emission scenarios, this CO_2 concentration is reached between 2049 and 2069 (Meinshausen et al., 2020).

3 Results

3.1 Structural influences on the strength of temperature and VPD effects

To evaluate how different model structural assumptions influence the apparent GPP response to temperature, we ran site-level simulations of K67 where we turned on and off photosynthetic temperature acclimation and plant hydraulics, resulting in a total of eight model configurations (see Methods). In observations at K67, light-saturated GPP declines by about 38% as temperature increases from 25°C to 32°C (Figure 1a). In all simulations of K67 under current conditions, light-saturated GPP declines as temperature increases, which is qualitatively consistent with observations (Figure 1a). The $CLM5_{AcclimAndHydro}$ and $CLM5_{HydroOnly}$ apparent GPP temperature response curves (green and blue dashed lines, respectively) most closely match this observed apparent GPP temperature response.

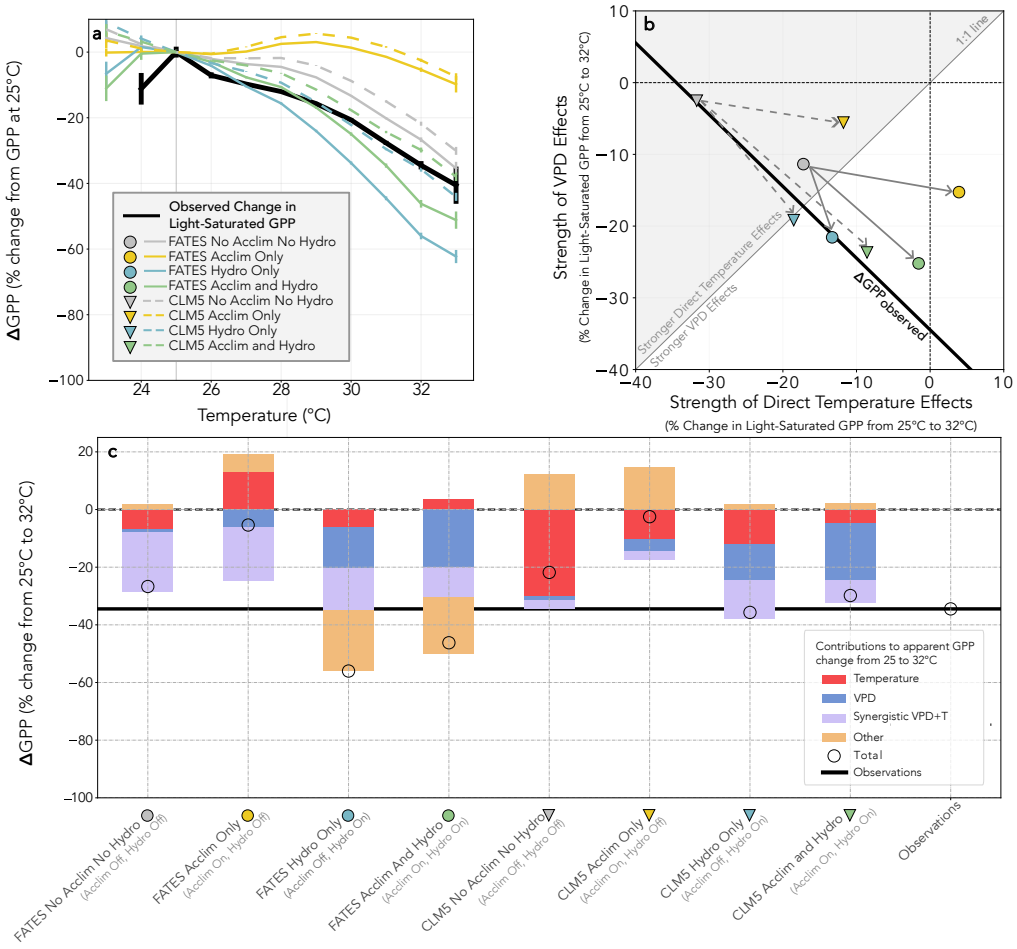

Figure 1. Process assumptions modify the strength of direct and indirect temperature effects. (a) The apparent light-saturated GPP response to temperature at the K67 site in observations and in different model configurations of FATES and CLM5. (b) The modeled strength of direct temperature effects and VPD effects, quantified as the percent change in light-saturated GPP from 25°C to 32°C as calculated from synthetic meteorology simulations. More negative values indicate stronger temperature and VPD effects on GPP. Nonlinear temperature-VPD effects are attributed equally to direct temperature and VPD effects, e.g. the temperature effect plotted on the x-axis is equal to the direct temperature effect plus $\frac{1}{2}$ of the nonlinear temperature-VPD synergistic effects. The gray 1:1 line delineates whether temperature or VPD effects are dominant. Points above the 1:1 line indicate that direct temperature effects are stronger than VPD effects, while points below the 1:1 line indicate that VPD effects are stronger. The black line marks the total apparent GPP response to temperature from 25°C to 32°C, which is an observational constraint if other meteorological effects are assumed to be zero. The observed ΔGPP is represented as a line to reflect ambiguity as to whether temperature or VPD effects are dominant. (c) The modeled strength of meteorological effects which contribute to the apparent GPP relationship with temperature, which is quantified as the percent change in light-saturated GPP from 25°C to 32°C as calculated from synthetic meteorology simulations. The total (circles) refers to the model output when actual site meteorology is used (equivalent to the sum of temperature, VPD, synergistic VPD+temperature, and other effects).

We then disentangled the direct and indirect effects of temperature and other meteorological drivers by running model experiments in which only one driver is allowed to vary at a time using synthetic meteorology. Across all model configurations, the apparent GPP response to temperature (defined in section 2.4, black horizontal line shows observations and black circles show modeled apparent GPP change) does not reflect the actual GPP response to direct temperature effects as quantified through direct modifications to meteorological forcing (Figure 1c). Rather, the apparent GPP response to temperature constitutes the combined effect of direct temperature effects (red bars), VPD effects (blue bars), synergistic VPD-temperature effects (purple bars), and other meteorological quantities that covary with temperature (orange bars).

The relative impact of temperature and VPD on GPP varies depending on model structural assumptions (Figure 1b-c). When neither photosynthetic temperature acclimation nor plant hydraulics are turned on, direct temperature effects in both FATES and CLM5 are stronger than VPD effects (gray circle and gray triangle, respectively, Figure 1b). Turning on photosynthetic temperature acclimation weakens direct temperature effects (moving from gray to yellow, Figure 1b), and adding plant hydraulics strengthens VPD effects (moving from gray to blue, Figure 1b). Weakening direct temperature effects and strengthening VPD effects have counteracting influences on the apparent GPP responses to temperature, such that turning on both photosynthetic temperature acclimation and plant hydraulics yields a combined temperature and VPD effect which is similar to the combined effect when both processes are turned off (Figure 1). Ultimately, however, this similar combined temperature and VPD effect is achieved through different partitioning between direct temperature and VPD effects under different model structural assumptions (moving from gray to green, Figure 1b). Model configurations with both processes turned off exist in the stronger direct temperature effects regime (above 1:1 line), while model configurations with both processes turned on exist in the stronger VPD effects regime (below 1:1 line, Figure 1b).

From Figures 1b and c, we find that model configurations that include plant hydraulics and temperature acclimation have different emergent strengths of VPD vs. temperature effects for the same overall combined VPD and temperature effect as configurations which do not include these processes. However, the synthetic meteorology simulations also demonstrate that temperature and VPD are not the sole drivers of the apparent GPP response to temperature. The apparent GPP response also is influenced by

other environmental factors (orange bars, Figure 1c). Turning on plant hydraulics also increases overall soil-plant water stress, especially in FATES (Figure S3), and this hydraulic stress contributes to apparent GPP declines with temperature because soil moisture is negatively correlated with temperature and VPD over seasonal timescales (Figure S2). In several model configurations ($\text{FATES}_{\text{AcclimOnly}}$, $\text{CLM5}_{\text{NoAcclimNoHydro}}$, $\text{CLM5}_{\text{AcclimOnly}}$) other environmental factors contribute to the apparent GPP response to temperature even when soil moisture, temperature, and VPD are held constant (blue lines in Figure S3), suggesting an influence of solar zenith angle or solar radiation.

Of the four FATES model configurations, $\text{FATES}_{\text{NoAcclimNoHydro}}$ (default FATES)'s apparent GPP temperature response is closest to the observed temperature response, followed by $\text{FATES}_{\text{AcclimAndHydro}}$. While $\text{FATES}_{\text{NoAcclimNoHydro}}$ and $\text{FATES}_{\text{AcclimAndHydro}}$ have similar combined temperature and VPD effects (Figure 1b), the apparent temperature response in $\text{FATES}_{\text{AcclimAndHydro}}$ deviates more from observations (Figure 1c) due to additional soil moisture stress (Figure S3). Observations do not directly measure how much different meteorological drivers contribute to this apparent GPP response to temperature, but previous work using analytical methods such as path analysis (Wu et al., 2017; Fu et al., 2018) and binned regression (Wu et al., 2017; Smith et al., 2020) suggest that at the K67 site VPD effects are stronger than direct temperature effects, indicating that model configurations in the stronger VPD effects regime are likely more consistent with observations.

3.2 Parametric influences on the strength of temperature and VPD effects

We ran a small perturbed parameter ensemble in $\text{FATES}_{\text{AcclimAndHydro}}$ to identify how plant functional traits influence the apparent GPP temperature response, and the relative strength of direct temperature and VPD effects. We found that the apparent GPP response to temperature is highly sensitive to plant functional parameters (Figure 2a). Our parameter ensemble yielded more variation in the strength of VPD effects (ranging from -27% to -12% from 25°C to 32°C) than variation in the strength of direct temperature effects (ranging from -6% to +1%) (Figure 2b). The maximum rate of Rubisco carboxylase activity (V_{cmax}) exerted a particularly strong control on VPD effects. Even though we sampled a broad parameter space, the $\text{FATES}_{\text{AcclimAndHydro}}$ model always hypothesized that VPD effects are stronger than direct temperature effects (Figure 2b),

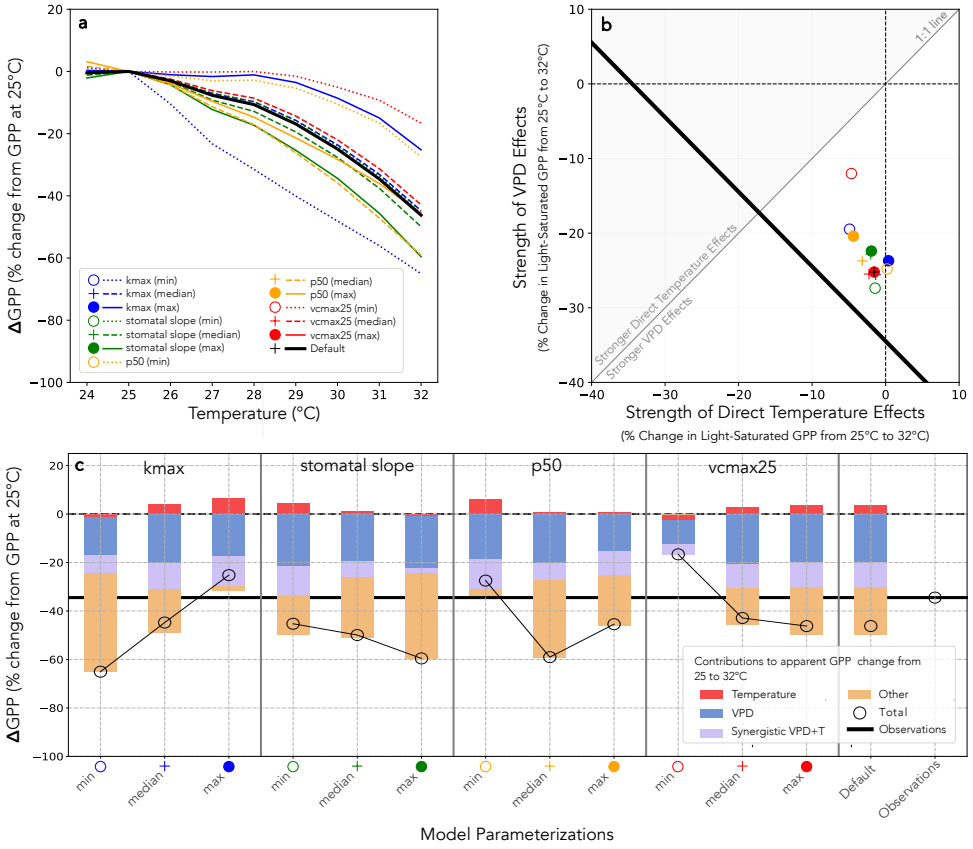

Figure 2. Plant functional traits modify the strength of direct and indirect temperature effects. The relative strength of direct temperature effects and VPD effects as in Figure 1, but for a perturbed parameter ensemble of $\text{FATES}_{\text{AcclimAndHydro}}$, varying kmax, stomatal slope, p50, and vcmax25.

suggesting that the qualitative dominance of direct temperature or VPD effects in models is relatively robust to parameter choice, and depends more on model structural assumptions (i.e. Figure 1b).

The large variation in the apparent GPP response to temperature across our ensemble was driven primarily by parameters' influence on the strength of other meteorological effects (orange bars, Figure 2c) such as soil moisture. Maximum hydraulic conductivity (kmax) exerted a particularly strong control over the apparent GPP response to temperature.

3.3 Apparent temperature responses across humidity gradients

In observations, B2 has a weaker apparent GPP response to temperature than natural tropical forest sites (Smith et al., 2020, Figure 3). We ran model simulations to test which assumptions are consistent with this cross-site variation in apparent GPP responses to temperature. When photosynthetic temperature acclimation and plant hydraulics are active in CLM5 ($CLM5_{AcclimAndHydro}$), modeled apparent GPP temperature response curves match observations relatively well at K67, MXTes, and B2 (Figure 1b), though GPP declines associated with increasing temperatures are slightly too weak at K67 and B2. As in observations, the K67 and B2 apparent temperature response curves begin to diverge from each other around 25°C. CLM5 is unable to capture this divergence in apparent temperature response curves without including temperature acclimation and plant hydraulics (compare Figures 3a and 3b). When these processes are turned off in $CLM5_{NoHydroNoAcclim}$, increasing temperatures are associated with modeled GPP declines that are too weak at K67 and too strong at B2.

In contrast, apparent GPP temperature response curves in $FATES_{AcclimAndHydro}$ do not perform well compared to B2 observations when photosynthetic temperature acclimation and plant hydraulics are active (Figure 3d). The $FATES_{AcclimAndHydro}$ apparent GPP temperature response fits observations reasonably well at K67, but B2 and MXTes GPP declines too much with increasing temperature in $FATES_{AcclimAndHydro}$. The strong apparent GPP temperature response in $FATES_{AcclimAndHydro}$at B2 is driven by soil moisture stress, as diagnosed by synthetic meteorology simulations with fully saturated soils (Figure S4). Changing B2 plant hydraulic traits so that B2 trees have higher maximum xylem hydraulic conductivity (16.04 kg/MPa/m/s compared to 3 kg/MPa/m/s) flattens the $FATES_{AcclimAndHydro}$ B2 apparent GPP temperature response by alleviating this water stress at B2 (dashed red line in Figure 3d). Turning off photosynthetic temperature acclimation and plant hydraulics also improves apparent GPP temperature response curves in FATES (Figure 1c). In $FATES_{NoAcclimNoHydro}$, modeled apparent GPP temperature response curves match observed response curves reasonably well, though GPP declines are slightly underestimated at K67 and overestimated at B2. B2 and K67 apparent temperature response curves diverge from each other at about 30°C in $FATES_{NoAcclimNoHydro}$.

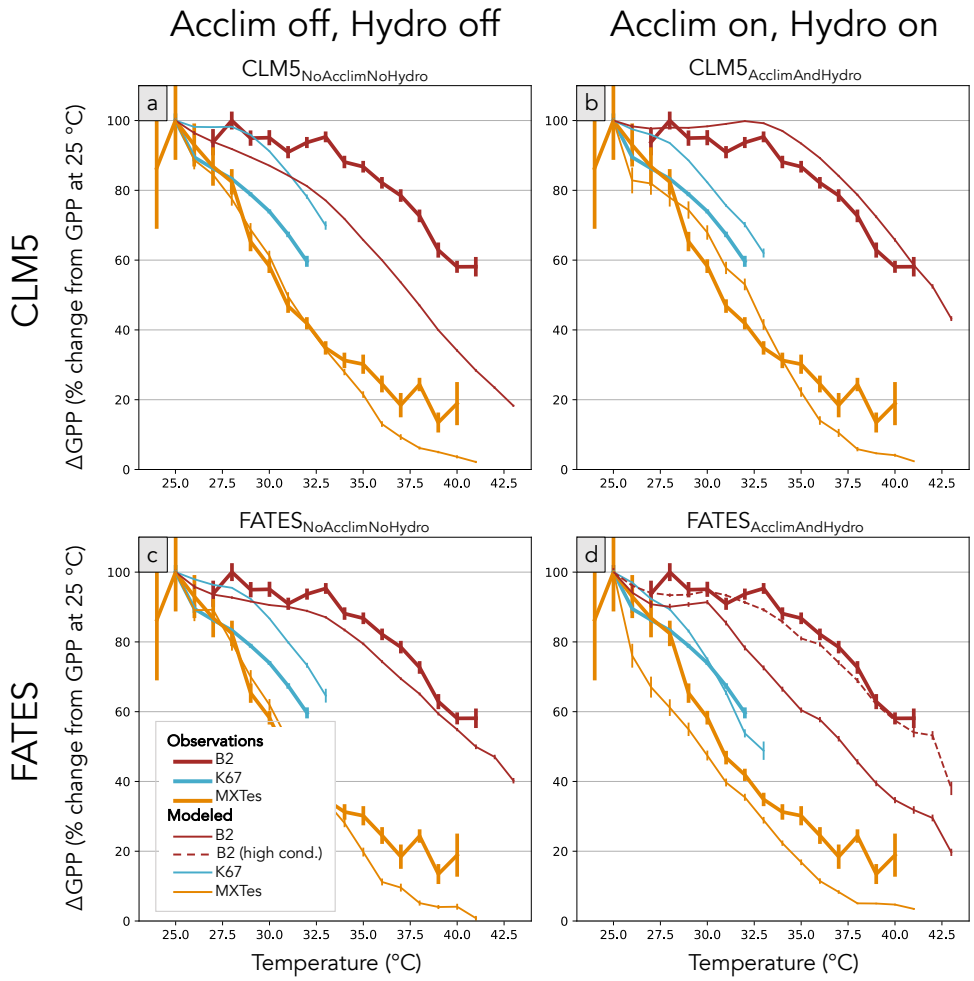

Figure 3. Observed and modeled apparent GPP responses to temperature at three tropical forest sites. Each panel compares observed and modeled apparent GPP responses to temperature for a different model configuration. In (a) and (c) photosynthetic temperature acclimation and plant hydraulics are turned off, and in (b) and (d), photosynthetic temperature acclimation and plant hydraulics are turned on. CLM5 is shown in (a) and (b), and FATES is shown in (c) and (d).

3.4 Different structural assumptions yield diverging projections

In the historical period, model assumptions consistent with strong direct temperature effects and weak VPD effects can yield a similar apparent GPP response to temperature as assumptions consistent with weak direct temperature effects and strong VPD effects (gray vs. green, Figure 1a). But our idealized climate treatment simulations demonstrate that these different assumptions yield diverging projections of ecosystem resilience to warming.

In models without photosynthetic temperature acclimation or plant hydraulics, light-saturated GPP decreases under an idealized increased temperature treatment (Figure 4a and c). In $\text{FATES}_{\text{NoAcclimNoHydro}}$ and $\text{CLM5}_{\text{NoAcclimNoHydro}}$, increasing temperature by 3°C decreases mean light-saturated GPP by 14% and 11%, respectively. These models are not sensitive to VPD changes, and are therefore not sensitive to different assumptions about relative humidity changes under warming (Figure 4a, Figure 4c, and Figure S5). In contrast, temperature increases drive minimal GPP changes in models with photosynthetic temperature acclimation and plant hydraulics turned on (Figure 4b and d). In $\text{FATES}_{\text{AcclimAndHydro}}$ and $\text{CLM5}_{\text{AcclimAndHydro}}$, the increased temperature treatment changes GPP by less than 3% as long as VPD is held constant at historical levels. These models are more sensitive to relative humidity changes under warming (Figure 4b, Figure 4d, and Figure S5). If the 3°C temperature increase is accompanied by 6% decrease in relative humidity, GPP decreases by 7 and 9%, respectively. If idealized climate treatments are accompanied by an increase in CO_2 concentration, GPP increases in all model configurations due to FATES and CLM's strong CO_2 fertilization effects. However, GPP increases more in $\text{FATES}_{\text{AcclimAndHydro}}$ and $\text{CLM5}_{\text{AcclimAndHydro}}$ than in $\text{FATES}_{\text{NoAcclimNoHydro}}$ and $\text{CLM5}_{\text{NoAcclimNoHydro}}$ (Figure S5).

Climate treatments' influence on the distributions of light-saturated GPP also differ between models. In $\text{FATES}_{\text{NoAcclimNoHydro}}$, $\text{CLM5}_{\text{NoAcclimNoHydro}}$, and $\text{CLM5}_{\text{AcclimAndHydro}}$, climate treatments shift the mean GPP but lead to minimal changes in the distribution of GPP around the mean. In $\text{FATES}_{\text{AcclimAndHydro}}$, climate treatments both shift the mean GPP and drive changes in the GPP distribution around the mean. Compared to observed light-saturated GPP, the mean light-saturated GPP for $\text{CLM5}_{\text{NoAcclimNoHydro}}$ and $\text{FATES}_{\text{AcclimAndHydro}}$ most closely match observations. There are biases in the GPP distributions in all models (Figure 4).

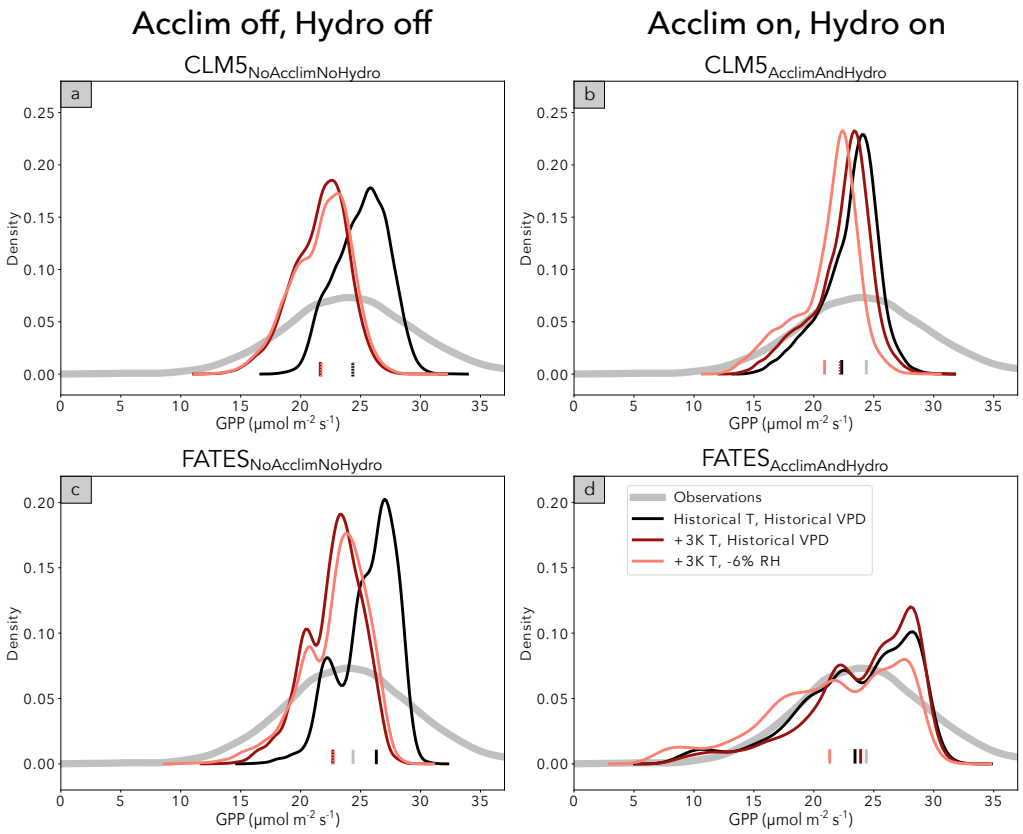

Figure 4. Shifts in the distribution of light-saturated photosynthesis at K67 under idealized climate treatments. Distributions of light-saturated GPP at K67 under different climate treatments for CLM5 (a-b) and FATES (c-d). In (a) and (c), photosynthetic temperature acclimation and plant hydraulics are turned off. In (b) and (d), photosynthetic temperature acclimation and plant hydraulics are turned on.

4 Discussion

4.1 Photosynthetic temperature acclimation and plant hydraulics

We found that both photosynthetic temperature acclimation and plant hydraulics govern the strength of direct temperature effects and VPD effects on photosynthesis (Figure 1), underscoring the importance of improving our scientific understanding and model representations of these processes. Models can achieve the same overall present day GPP response to temperature and VPD by excluding both of these processes (which yields stronger direct temperature effects) or by including both of these processes (which yields stronger VPD effects). However, these two sets of assumptions yield diverging predictions of ecosystem resilience to warming (Figure 4). Assumptions consistent with stronger direct temperature effects resulted in larger GPP declines under warming, while assumptions consistent with stronger VPD effects resulted in more resilient GPP under warming. This suggests that the relative strength of direct temperature vs. VPD effects on GPP in the present day may be a useful diagnostic for GPP responses to future warming. It has long been recognized that land surface models tend to fit historical data relatively well, but then diverge from each other under future conditions (Friedlingstein et al., 2006, 2013; Lovenduski & Bonan, 2017; Booth et al., 2017), in part due to the challenge of equifinality (J. Tang & Zhuang, 2008; Fisher & Koven, 2020). This study identifies that the tradeoff between weak VPD effects and strong temperature effects vs. strong VPD effects and weak temperature effects is an important axis along which compensating errors may occur in models.

Photosynthetic temperature acclimation and plant hydraulics are well established processes with important effects on ecosystem functioning, so broadly we expect that model configurations that include these processes should be more realistic than model configurations which exclude them. Previous observationally-based studies indicate that VPD effects are stronger than direct temperature effects at K67 in particular (Wu et al., 2017; Fu et al., 2018; Smith et al., 2020), and at tropical forests in general (Smith et al., 2020). This suggests that structural assumptions that put models in the stronger VPD effect regime are more realistic, and that models without photosynthetic temperature acclimation or plant hydraulics may match observations by assuming unrealistically strong direct temperature effects. Most land models used to quantify carbon cycle responses to warming as part of the Coupled Model Intercomparison Project Phase 6 (CMIP6) do

not include photosynthetic temperature acclimation or plant hydraulics (Table S1), so we hypothesize that such land models may overestimate the strength of direct temperature effects and underestimate VPD effects. Given that the present-day partitioning between temperature and VPD effects may be a useful diagnostic for model GPP sensitivity to warming, we call for more modeling centers to use synthetic meteorology methods to explicitly quantify how much modeled apparent GPP responses to temperature in the present day are driven by direct temperature effects, VPD effects, and other meteorological drivers.

In this study we focus on how photosynthetic temperature acclimation and plant hydraulics influence GPP responses to warming, but we also note that photosynthetic temperature acclimation and plant hydraulics can influence tropical carbon pool responses to concurrent changes in atmospheric CO_2 concentration, precipitation, and other environmental conditions. For example, Lombardozzi et al. (2015) found that turning on photosynthetic and respiratory temperature acclimation yielded a smaller tropical carbon pool increase from 1850 to 2100, compared to simulations when these processes were turned off. This was attributed to the fact that 1850 tropical carbon pools were larger in simulations that included temperature acclimation, but the rate of ecosystem-level carbon accumulation slowed by the end of the 21st century due to limitation of another environmental quantity (e.g. nutrient or water limitation).

4.2 Plant functional traits

We found that plant functional traits control the strength of VPD and temperature effects (Figure 2), which means that the strength of these effects can differ across time and space due to variation in tropical forest functional composition. This poses a challenge for modeling tropical forest responses at a regional to pan-tropical scale, because doing so will require representing the diversity of plant functional traits which can vary widely both within an ecosystem and geographically. This, paired with the fact that hydraulic trait data for tropical forests is limited, motivates further data collection of tropical tree hydraulic trait data through field campaigns (Tavares et al., 2023; Christoffersen et al., 2016) and satellite-based methods (e.g. Liu et al., 2021). For example, our perturbed parameter ensemble demonstrated that the apparent GPP response to temperature is highly sensitive to plants' stem maximum hydraulic capacity. However, a previous meta-analysis identified less than 300 observations of this trait for tropical trees

(Christoffersen, 2021). Collecting more hydraulic trait data, and developing methods for estimating hydraulic traits based on correlations with environmental conditions or more easily collected plant traits, will enable better model representation of ecosystem photosynthetic responses to temperature, VPD, and soil moisture. Our results also suggest that GPP sensitivities to environmental changes are influenced by variation in plant traits within an ecosystem, due to both variation across trees (e.g. X. Xu et al., 2016) and vertical variation in plant traits and forest microclimates (Vinod et al., 2023).

Previous studies have documented differing strengths of VPD and temperature effects on GPP across tropical forest sites (Fu et al., 2018), and we demonstrate here that this variation could be partially due to inter-site variation in plant functional traits. Additionally, tropical forest functional composition can change in response to changing climate, thereby driving shifts in tropical forest GPP sensitivities to VPD, temperature, and soil moisture. This nonstationarity in time points to the importance of accounting for dynamic ecosystem functional assembly (Fisher et al., 2015) when predicting tropical forest photosynthesis under novel climates on longer timescales.

4.3 Multiple hypotheses consistent with apparent GPP responses to temperature at Biosphere 2

From observations alone, it is challenging to identify which unique features of Biosphere 2 (see section 2.1) enable the site to maintain high photosynthetic rates even at high temperatures. Broadly, we expect that models should be able to represent all sites using the same physiological rules, and that B2's shallower apparent GPP temperature response curve could be due to (1) environmental and/or (2) biological differences between B2 and natural forest sites. If environmental differences are the primary driver of the different apparent GPP temperature responses across sites, we would expect that models could represent cross-site variation in GPP temperature response curves using one common set of plant traits for all sites. If biological differences are the primary driver of the different apparent GPP temperature responses across sites, it would be necessary to vary plant traits across sites.

Our results indicate that we cannot currently distinguish between these two perspectives (Figure 3). Simulations in CLM suggest that the different apparent GPP temperature responses between B2 and the natural tropical forest sites can be explained by

environmental differences, but only if both plant hydraulics and photosynthetic temperature acclimation processes are turned on. Considering only CLM simulations would therefore support the idea that $CLM5_{AcclimAndHydro}$ includes more realistic set of physiological rules than $CLM5_{NoAcclimNoHydro}$, because only $CLM5_{AcclimAndHydro}$ is able to capture the variation in GPP temperature responses across humidity gradients.

FATES simulations, however, support the alternative hypothesis that biological differences contribute to the different apparent GPP temperature responses across sites. In $FATES_{AcclimAndHydro}$, environmental differences alone cannot explain the differences in apparent GPP temperature responses across sites because $FATES_{AcclimAndHydro}$ cannot capture the shallower temperature response curve at B2. However, $FATES_{AcclimAndHydro}$ can capture the variation in GPP temperature responses across sites if B2 trees have higher maximum hydraulic conductivity. This change reduces (but does not eliminate) large biases in FATES' modeled leaf water potential compared to observations (Figure S6) and aligns with the fact that trees at B2 have lower wood density than most tropical trees, which is associated with higher maximum xylem conductivity (Christoffersen et al., 2016). Prior studies also suggest that the functional composition of B2 may differ from natural tropical forests. For example, over the last twenty years the percentage of trees at B2 that emit isoprene has increased (Taylor et al., 2018), which suggests a shift towards higher community-weighted photosynthetic rates at high temperatures (Taylor et al., 2019).

The different GPP responses between $FATES_{AcclimAndHydro}$ and $CLM5_{AcclimAndHydro}$ at B2 demonstrate that photosynthetic responses to temperature and VPD are not simply determined by whether or not models include plant hydraulics. The implementation of plant hydraulic processes (which differs between FATES and CLM) matters, as do the specific values of plant hydraulic traits. We also note that soil hydrology is important for capturing the temporal variation in plant leaf water potential, and can therefore also influence photosynthetic responses to VPD. The water transport through plants depends on soil water potential, so if models have oversimplified soil hydrology, soil hydrology biases can lead to inaccurate leaf water potential and water fluxes (Ivanov et al., 2012; Restrepo-Coupe et al., 2017) even if models were to perfectly represent plant hydraulics.

4.4 Drivers of GPP variation on different timescales

Predicting tropical forest GPP responses to a warming climate will require understanding biotic and abiotic controls on photosynthesis across a range of timescales, from hours to centuries, and accurately representing these processes in models. This paper focuses on variation in hourly light-saturated GPP, which is the timescale at which land surface models are perhaps most likely to match observations because land surface models have represented instantaneous leaf-level responses to environmental conditions for decades (Fisher and Koven 2020). The fact that structural assumptions not included in many land models can influence photosynthesis at this timescale underscores the importance of doing this kind of test. Our model simulations did not represent temporal variation in leaf area, leaf age, or plant functional composition, which is a reasonable simplification for this study because on hourly timescales GPP is primarily driven by environmental rather than biotic variability (Wu et al., 2017). However, while the data is hourly, trends may in part be related to factors varying at seasonal timescales. For example, if GPP decreases with temperature and the true driver of this relationship were soil moisture, that would be because higher temperatures are occurring during the dry season when soil moisture is lower, creating a spurious correlation that occurs over seasonal timescales.

Ultimately, however, it is necessary to compare models and observations at all timescales, and biotic variation is increasingly important when considering GPP variability beyond hourly timescales (Wu et al., 2017). Mechanistically representing the processes affecting canopy light-use efficiency, such as plant carbon allocation and leaf turnover, will be essential for capturing monthly and interannual GPP responses to temperature and VPD. Previous work has found that forest photosynthetic capacity increases in the dry season (Wu et al., 2017; Albert et al., 2018; Lopes et al., 2016; A. C. I. Tang et al., 2019), and that on monthly timescales VPD increases may increase photosynthesis by stimulating flushing of new leaves (Restrepo-Coupe et al., 2013). Additionally, representing how environmental change alters forest functional composition is an important process on decadal to centennial timescales.

Another limitation of our modeling approach is that we represented each site using a single plant functional type, and therefore did not represent within-site functional diversity. Previous work has demonstrated that diversity in plant traits is an important

control on ecosystem responses to water stress (Werner et al., 2021) and seasonal to interannual variation in ecosystem functioning (X. Xu et al., 2016). Our simulations also did not represent vertical variations in plant traits and forest microclimates, which previous work suggests is important for forest responses (Smith et al., 2019), but is often insufficiently represented in models (Vinod et al., 2023). We encourage future work to expand on this study by quantifying how functional diversity and seasonal to interannual biotic variations influence GPP responses to temperature and VPD effects at multiple timescales.

5 Conclusions

We demonstrated that plant functional parameters and structural assumptions about photosynthetic temperature acclimation and plant hydraulics control the strength of temperature and VPD effects on tropical forest photosynthesis. This led us to identify a novel axis along which compensating errors can occur in models – models can match observed apparent ecosystem-level photosynthesis responses to temperature by excluding both processes (which yields stronger direct temperature effects) or by including both processes (which yields stronger VPD effects). However, these two sets of assumptions yield diverging predictions of ecosystem resilience to warming, underscoring the importance of improving our scientific understanding and model representations of these processes. This study also demonstrates the challenges of disentangling temperature vs. VPD effects from observational data alone. Developing further observational constraints on the partitioning between temperature vs. VPD influences in the historical period should be a future research priority, as should using those observational constraints to evaluate model performance.

Author Contributions

CMZ, CDK, and ALSS conceptualized the research project, developed the methodology, and administered the project. ALSS and CDK supervised the project and provided computing resources. CMZ acquired the primary funding, ran model experiments, performed analysis, prepared visualizations, and wrote the original draft. ALSS, CDK, MNS, and TCT reviewed and edited writing. MNS and TCT collected observational data. CMZ and CDK developed code used in this research. CMZ, CDK, MNS, and TCT curated data.

Acknowledgements

CMZ was supported by the U.S. Department of Energy (DOE) Computational Science Graduate Fellowship (DE-SC0020347). ALSS and CMZ were supported by the DOE Regional and Global Model Analysis Program (DE-SC0021209) and the National Science Foundation (NSF) grant AGS-1553715 to the University of Washington. CDK was supported by the Next Generation Ecosystem Experiments-Tropics project, funded by the DOE, Office of Science, Office of Biological and Environmental Research. MNS was supported by NSF DEB grant 1950080 to Michigan State University (MSU). TCT was supported by NSF grant 2111028 to the University of Michigan. We thank FLUXNET, Ameriflux, and Rafael Rosolem for providing publicly accessible net ecosystem exchange data and gap-filled meteorological data. We also thank all scientists, software engineers, and administrators who contributed to the development of FATES and CLM5.

Conflict of Interest Statement

The authors declare that they have no conflicts of interest.

Open Research

The original data for this study are all publicly available. The observational gap-filled meteorological data and net ecosystem exchange (NEE) data are available for K67 at `https://ameriflux.lbl.gov/sites/siteinfo/BR-Sa1`, and for B2 and MXTes at `https://github.com/m-n-smith/B2-temp-paper-datasets`. The output of all model simulations used in this paper is available in the Dryad Digital Repository at `https://doi.org/10.5061/dryad.wdbrv15w2`.

References

Albert, L. P., Wu, J., Prohaska, N., de Camargo, P. B., Huxman, T. E., Tribuzy, E. S., ... Saleska, S. R. (2018). Age-dependent leaf physiology and consequences for crown-scale carbon uptake during the dry season in an Amazon evergreen forest. *New Phytologist*, *219*(3), 870–884. doi: 10.1111/nph.15056

Arain, M. A., James Shuttleworth, W., Farnsworth, B., Adams, J., & Lutfi Sen, O. (2000, February). Comparing micrometeorology of rain forests in Biosphere-2 and Amazon basin. *Agricultural and Forest Meteorology*, *100*(4), 273–289. doi:

10.1016/S0168-1923(99)00153-7

Ball, J. T., Woodrow, I. E., & Berry, J. A. (1987). A Model Predicting Stomatal Conductance and its Contribution to the Control of Photosynthesis under Different Environmental Conditions. In J. Biggins (Ed.), *Progress in Photosynthesis Research: Volume 4 Proceedings of the VIIth International Congress on Photosynthesis Providence, Rhode Island, USA, August 10–15, 1986* (pp. 221–224). Dordrecht: Springer Netherlands. doi: 10.1007/978-94-017-0519-6_48

Booth, B. B. B., Harris, G. R., Murphy, J. M., House, J. I., Jones, C. D., Sexton, D., & Sitch, S. (2017, April). Narrowing the Range of Future Climate Projections Using Historical Observations of Atmospheric CO2. *Journal of Climate*, *30*(8), 3039–3053. doi: 10.1175/JCLI-D-16-0178.1

Byrne, M. P., & O'Gorman, P. A. (2018, May). Trends in continental temperature and humidity directly linked to ocean warming. *Proceedings of the National Academy of Sciences*, *115*(19), 4863–4868. doi: 10.1073/pnas.1722312115

Christoffersen, B. O. (2021). Pantropical tropical tree xylem hydraulic functional traits, 1991 - 2013. 1.0. NGEE Tropics Data Collection. doi: http://dx.doi.org/10.15486/ngt/1581482

Christoffersen, B. O., Gloor, M., Fauset, S., Fyllas, N. M., Galbraith, D. R., Baker, T. R., ... Meir, P. (2016, November). Linking hydraulic traits to tropical forest function in a size-structured and trait-driven model (TFS v.1-Hydro). *Geoscientific Model Development*, *9*(11), 4227–4255. doi: 10.5194/gmd-9-4227-2016

Doughty, C. E., & Goulden, M. L. (2008). Are tropical forests near a high temperature threshold? *Journal of Geophysical Research: Biogeosciences*, *113*(G1). doi: 10.1029/2007JG000632

Doughty, C. E., Keany, J. M., Wiebe, B. C., Rey-Sanchez, C., Carter, K. R., Middleby, K. B., ... Fisher, J. B. (2023, September). Tropical forests are approaching critical temperature thresholds. *Nature*, *621*(7977), 105–111. doi: 10.1038/s41586-023-06391-z

Duffy, K. A., Schwalm, C. R., Arcus, V. L., Koch, G. W., Liang, L. L., & Schipper, L. A. (2021, January). How close are we to the temperature tipping point of the terrestrial biosphere? *Science Advances*, *7*(3), eaay1052. doi: 10.1126/sciadv.aay1052

Dusenge, M. E., Duarte, A. G., & Way, D. A. (2019). Plant carbon metabolism and climate change: elevated CO2 and temperature impacts on photosynthesis, photorespiration and respiration. *New Phytologist*, *221*(1), 32–49. doi: 10.1111/nph.15283

Fisher, R. A., & Koven, C. D. (2020). Perspectives on the Future of Land Surface Models and the Challenges of Representing Complex Terrestrial Systems. *Journal of Advances in Modeling Earth Systems*, *12*(4), e2018MS001453. doi: 10.1029/2018MS001453

Fisher, R. A., Muszala, S., Verteinstein, M., Lawrence, P., Xu, C., McDowell, N. G., ... Bonan, G. (2015, November). Taking off the training wheels: the properties of a dynamic vegetation model without climate envelopes, CLM4.5(ED). *Geoscientific Model Development*, *8*(11), 3593–3619. doi: 10.5194/gmd-8-3593-2015

Friedlingstein, P., Cox, P., Betts, R., Bopp, L., von Bloh, W., Brovkin, V., ... Zeng, N. (2006, July). Climate–Carbon Cycle Feedback Analysis: Results from the C4MIP Model Intercomparison. *Journal of Climate*, *19*(14), 3337–3353. doi: 10.1175/JCLI3800.1

Friedlingstein, P., Meinshausen, M., Arora, V. K., Jones, C. D., Anav, A., Liddicoat, S. K., & Knutti, R. (2013, September). Uncertainties in CMIP5 Climate Projections due to Carbon Cycle Feedbacks. *Journal of Climate*, *27*(2), 511–526. doi: 10.1175/JCLI-D-12-00579.1

Fu, Z., Gerken, T., Bromley, G., Araújo, A., Bonal, D., Burban, B., ... Stoy, P. C. (2018, December). The surface-atmosphere exchange of carbon dioxide in tropical rainforests: Sensitivity to environmental drivers and flux measurement methodology. *Agricultural and Forest Meteorology*, *263*, 292–307. doi: 10.1016/j.agrformet.2018.09.001

Galbraith, D., Levy, P. E., Sitch, S., Huntingford, C., Cox, P., Williams, M., & Meir, P. (2010). Multiple mechanisms of Amazonian forest biomass losses in three dynamic global vegetation models under climate change. *New Phytologist*, *187*(3), 647–665. doi: 10.1111/j.1469-8137.2010.03350.x

Grossiord, C., Buckley, T. N., Cernusak, L. A., Novick, K. A., Poulter, B., Siegwolf, R. T. W., ... McDowell, N. G. (2020). Plant responses to rising vapor pressure deficit. *New Phytologist*, *226*(6), 1550–1566. doi: 10.1111/nph.16485

Huang, M., Piao, S., Ciais, P., Peñuelas, J., Wang, X., Keenan, T. F., ... Janssens, I. A. (2019, May). Air temperature optima of vegetation productivity across global biomes. *Nature Ecology & Evolution*, *3*(5), 772–779. doi: 10.1038/s41559-019-0838-x

Hutyra, L. R., Munger, J. W., Saleska, S. R., Gottlieb, E., Daube, B. C., Dunn, A. L., ... Wofsy, S. C. (2007). Seasonal controls on the exchange of carbon and water in an Amazonian rain forest. *Journal of Geophysical Research: Biogeosciences*, *112*(G3). doi: 10.1029/2006JG000365

Ivanov, V. Y., Hutyra, L. R., Wofsy, S. C., Munger, J. W., Saleska, S. R., de Oliveira Jr., R. C., & de Camargo, P. B. (2012). Root niche separation can explain avoidance of seasonal drought stress and vulnerability of overstory trees to extended drought in a mature Amazonian forest. *Water Resources Research*, *48*(12). doi: 10.1029/2012WR011972

Kattge, J., & Knorr, W. (2007). Temperature acclimation in a biochemical model of photosynthesis: a reanalysis of data from 36 species. *Plant, Cell & Environment*, *30*(9), 1176–1190. doi: 10.1111/j.1365-3040.2007.01690.x

Kennedy, D., Swenson, S., Oleson, K. W., Lawrence, D. M., Fisher, R., Costa, A. C. L. d., & Gentine, P. (2019). Implementing Plant Hydraulics in the Community Land Model, Version 5. *Journal of Advances in Modeling Earth Systems*, *11*(2), 485–513. doi: https://doi.org/10.1029/2018MS001500

Koven, C. D., Knox, R. G., Fisher, R. A., Chambers, J. Q., Christoffersen, B. O., Davies, S. J., ... Xu, C. (2020, June). Benchmarking and parameter sensitivity of physiological and vegetation dynamics using the Functionally Assembled Terrestrial Ecosystem Simulator (FATES) at Barro Colorado Island, Panama. *Biogeosciences*, *17*(11), 3017–3044. doi: 10.5194/bg-17-3017-2020

Kumarathunge, D. P., Medlyn, B. E., Drake, J. E., Tjoelker, M. G., Aspinwall, M. J., Battaglia, M., ... Way, D. A. (2019). Acclimation and adaptation components of the temperature dependence of plant photosynthesis at the global scale. *New Phytologist*, *222*(2), 768–784. doi: https://doi.org/10.1111/nph.15668

Lawrence, D. M., Fisher, R. A., Koven, C. D., Oleson, K. W., Swenson, S. C., Bonan, G., ... Zeng, X. (2019). The Community Land Model Version 5: Description of New Features, Benchmarking, and Impact of Forcing Uncertainty. *Journal of Advances in Modeling Earth Systems*, *11*, 4245–4287. doi:

10.1029/2018MS001583

Li, Y., Baker, J. C. A., Brando, P. M., Hoffman, F. M., Lawrence, D. M., Morton, D. C., ... Randerson, J. T. (2023, September). Future increases in Amazonia water stress from CO2 physiology and deforestation. *Nature Water*, *1*(9), 769–777. doi: 10.1038/s44221-023-00128-y

Liu, Y., Holtzman, N. M., & Konings, A. G. (2021, May). Global ecosystem-scale plant hydraulic traits retrieved using model–data fusion. *Hydrology and Earth System Sciences*, *25*(5), 2399–2417. doi: 10.5194/hess-25-2399-2021

Lloyd, J., & Farquhar, G. D. (2008, May). Effects of rising temperatures and [CO2] on the physiology of tropical forest trees. *Philosophical Transactions of the Royal Society B: Biological Sciences*, *363*(1498), 1811–1817. doi: 10.1098/rstb.2007.0032

Lombardozzi, D. L., Bonan, G. B., Smith, N. G., Dukes, J. S., & Fisher, R. A. (2015). Temperature acclimation of photosynthesis and respiration: A key uncertainty in the carbon cycle-climate feedback. *Geophysical Research Letters*, *42*(20), 8624–8631. doi: https://doi.org/10.1002/2015GL065934

Lopes, A. P., Nelson, B. W., Wu, J., Graça, P. M. L. d. A., Tavares, J. V., Prohaska, N., ... Saleska, S. R. (2016, September). Leaf flush drives dry season greenup of the Central Amazon. *Remote Sensing of Environment*, *182*, 90–98. doi: 10.1016/j.rse.2016.05.009

Lovenduski, N. S., & Bonan, G. B. (2017, April). Reducing uncertainty in projections of terrestrial carbon uptake. *Environmental Research Letters*, *12*(4), 044020. doi: 10.1088/1748-9326/aa66b8

Mau, A. C., Reed, S. C., Wood, T. E., & Cavaleri, M. A. (2018, January). Temperate and Tropical Forest Canopies are Already Functioning beyond Their Thermal Thresholds for Photosynthesis. *Forests*, *9*(1), 47. doi: 10.3390/f9010047

Medlyn, B. E., Duursma, R. A., Eamus, D., Ellsworth, D. S., Prentice, I. C., Barton, C. V. M., ... Wingate, L. (2011). Reconciling the optimal and empirical approaches to modelling stomatal conductance. *Global Change Biology*, *17*(6), 2134–2144. doi: 10.1111/j.1365-2486.2010.02375.x

Meinshausen, M., Nicholls, Z. R. J., Lewis, J., Gidden, M. J., Vogel, E., Freund, M., ... Wang, R. H. J. (2020, August). The shared socio-economic pathway (SSP) greenhouse gas concentrations and their extensions to 2500. *Geoscientific Model*

Development, *13*(8), 3571–3605. doi: 10.5194/gmd-13-3571-2020

Pastorello, G., Trotta, C., Canfora, E., Chu, H., Christianson, D., Cheah, Y.-W., ... Papale, D. (2020, July). The FLUXNET2015 dataset and the ONEFlux processing pipeline for eddy covariance data. *Scientific Data*, *7*(1), 225. doi: 10.1038/s41597-020-0534-3

Perez-Ruiz, E. R., Garatuza-Payan, J., Watts, C. J., Rodriguez, J. C., Yepez, E. A., & Scott, R. L. (2010, May). Carbon dioxide and water vapour exchange in a tropical dry forest as influenced by the North American Monsoon System (NAMS). *Journal of Arid Environments*, *74*(5), 556–563. doi: 10.1016/j.jaridenv.2009.09.029

Rascher, U., Bobich, E. G., Lin, G. H., Walter, A., Morris, T., Naumann, M., ... Berry, J. A. (2004). Functional diversity of photosynthesis during drought in a model tropical rainforest – the contributions of leaf area, photosynthetic electron transport and stomatal conductance to reduction in net ecosystem carbon exchange. *Plant, Cell & Environment*, *27*(10), 1239–1256. doi: https://doi.org/10.1111/j.1365-3040.2004.01231.x

Restrepo-Coupe, N., da Rocha, H. R., Hutyra, L. R., da Araujo, A. C., Borma, L. S., Christoffersen, B., ... Saleska, S. R. (2013, December). What drives the seasonality of photosynthesis across the Amazon basin? A cross-site analysis of eddy flux tower measurements from the Brasil flux network. *Agricultural and Forest Meteorology*, *182-183*, 128–144. doi: 10.1016/j.agrformet.2013.04.031

Restrepo-Coupe, N., Levine, N. M., Christoffersen, B. O., Albert, L. P., Wu, J., Costa, M. H., ... Saleska, S. R. (2017). Do dynamic global vegetation models capture the seasonality of carbon fluxes in the Amazon basin? A data-model intercomparison. *Global Change Biology*, *23*(1), 191–208. doi: https://doi.org/10.1111/gcb.13442

Rosolem, R., Shuttleworth, W. J., Zeng, X., Saleska, S. R., & Huxman, T. E. (2010). Land surface modeling inside the Biosphere 2 tropical rain forest biome. *Journal of Geophysical Research: Biogeosciences*, *115*(G4). doi: https://doi.org/10.1029/2010JG001443

Rowland, L., Harper, A., Christoffersen, B. O., Galbraith, D. R., Imbuzeiro, H. M. A., Powell, T. L., ... Williams, M. (2015, April). Modelling climate change responses in tropical forests: similar productivity estimates across five models,

but different mechanisms and responses. *Geoscientific Model Development*, *8*(4), 1097–1110. doi: 10.5194/gmd-8-1097-2015

Sanchez-Mejia, Z. M., Garatuza Payan, J., Yepez, E. A., Perez Ruiz, E. R., Peñuelas Rubio, O., Serrano Grijalva, L., ... Siqueiros, E. (2021, March). *Floristic composition surrounding the footprint of eddy covariance and micrometeorology tower in the tropical dry forest, Tesopaco, Sonora (México).*

Santos, V. A. H. F. d., Ferreira, M. J., Rodrigues, J. V. F. C., Garcia, M. N., Ceron, J. V. B., Nelson, B. W., & Saleska, S. R. (2018). Causes of reduced leaf-level photosynthesis during strong El Niño drought in a Central Amazon forest. *Global Change Biology*, *24*(9), 4266–4279. doi: 10.1111/gcb.14293

Slot, M., Garcia, M. N., & Winter, K. (2016, March). Temperature response of CO2 exchange in three tropical tree species. *Functional Plant Biology*, *43*(5), 468–478. doi: 10.1071/FP15320

Slot, M., & Winter, K. (2016). The Effects of Rising Temperature on the Ecophysiology of Tropical Forest Trees. In G. Goldstein & L. S. Santiago (Eds.), *Tropical Tree Physiology: Adaptations and Responses in a Changing Environment* (pp. 385–412). Cham: Springer International Publishing. doi: 10.1007/978-3-319-27422-5_18

Smith, M. N., Stark, S. C., Taylor, T. C., Ferreira, M. L., de Oliveira, E., Restrepo-Coupe, N., ... Saleska, S. R. (2019). Seasonal and drought-related changes in leaf area profiles depend on height and light environment in an Amazon forest. *New Phytologist*, *222*(3), 1284–1297. doi: 10.1111/nph.15726

Smith, M. N., Taylor, T. C., van Haren, J., Rosolem, R., Restrepo-Coupe, N., Adams, J., ... Saleska, S. R. (2020, October). Empirical evidence for resilience of tropical forest photosynthesis in a warmer world. *Nature Plants*, *6*(10), 1225–1230. doi: 10.1038/s41477-020-00780-2

Tan, Z.-H., Zeng, J., Zhang, Y.-J., Slot, M., Gamo, M., Hirano, T., ... Restrepo-Coupe, N. (2017, May). Optimum air temperature for tropical forest photosynthesis: mechanisms involved and implications for climate warming. *Environmental Research Letters*, *12*(5), 054022. doi: 10.1088/1748-9326/aa6f97

Tang, A. C. I., Stoy, P. C., Hirata, R., Musin, K. K., Aeries, E. B., Wenceslaus, J., ... Melling, L. (2019, September). The exchange of water and energy between a tropical peat forest and the atmosphere: Seasonal trends and comparison against

other tropical rainforests. *Science of The Total Environment*, *683*, 166–174. doi: 10.1016/j.scitotenv.2019.05.217

Tang, J., & Zhuang, Q. (2008). Equifinality in parameterization of process-based biogeochemistry models: A significant uncertainty source to the estimation of regional carbon dynamics. *Journal of Geophysical Research: Biogeosciences*, *113*(G4). doi: 10.1029/2008JG000757

Tavares, J. V., Oliveira, R. S., Mencuccini, M., Signori-Müller, C., Pereira, L., Diniz, F. C., ... Galbraith, D. R. (2023, May). Basin-wide variation in tree hydraulic safety margins predicts the carbon balance of Amazon forests. *Nature*, *617*(7959), 111–117. doi: 10.1038/s41586-023-05971-3

Taylor, T. C., McMahon, S. M., Smith, M. N., Boyle, B., Violle, C., van Haren, J., ... Saleska, S. R. (2018). Isoprene emission structures tropical tree biogeography and community assembly responses to climate. *New Phytologist*, *220*(2), 435–446. doi: 10.1111/nph.15304

Taylor, T. C., Smith, M. N., Slot, M., & Feeley, K. J. (2019). The capacity to emit isoprene differentiates the photosynthetic temperature responses of tropical plant species. *Plant, Cell & Environment*, *42*(8), 2448–2457. doi: 10.1111/pce.13564

Vargas-G, G., & Cordero, R. A. (2013, October). Photosynthetic responses to temperature of two tropical rainforest tree species from Costa Rica. *Trees*, *27*(5), 1261–1270. doi: 10.1007/s00468-013-0874-0

Vinod, N., Slot, M., McGregor, I. R., Ordway, E. M., Smith, M. N., Taylor, T. C., ... Anderson-Teixeira, K. J. (2023). Thermal sensitivity across forest vertical profiles: patterns, mechanisms, and ecological implications. *New Phytologist*, *237*(1), 22–47. doi: 10.1111/nph.18539

Werner, C., Meredith, L. K., Ladd, S. N., Ingrisch, J., Kübert, A., Haren, J. v., ... Williams, J. (2021, December). Ecosystem fluxes during drought and recovery in an experimental forest. *Science*. doi: 10.1126/science.abj6789

Wu, J., Guan, K., Hayek, M., Restrepo-Coupe, N., Wiedemann, K. T., Xu, X., ... Saleska, S. R. (2017). Partitioning controls on Amazon forest photosynthesis between environmental and biotic factors at hourly to interannual timescales. *Global Change Biology*, *23*(3), 1240–1257. doi: https://doi.org/10.1111/gcb.13509

Xu, C., Christoffersen, B., Robbins, Z., Knox, R., Fisher, R. A., Chitra-Tarak, R., ... McDowell, N. (2023, November). Quantification of hydraulic trait control

on plant hydrodynamics and risk of hydraulic failure within a demographic structured vegetation model in a tropical forest (FATES–HYDRO V1.0). *Geoscientific Model Development*, *16*(21), 6267–6283. doi: 10.5194/gmd-16-6267-2023

Xu, X., Medvigy, D., Powers, J. S., Becknell, J. M., & Guan, K. (2016). Diversity in plant hydraulic traits explains seasonal and inter-annual variations of vegetation dynamics in seasonally dry tropical forests. *New Phytologist*, *212*(1), 80–95. doi: 10.1111/nph.14009

Yepez, E. A., & Garatuza, J. (2021, January). *AmeriFlux FLUXNET-1F MX-Tes Tesopaco, secondary tropical dry forest* (Tech. Rep.). Lawrence Berkeley National Lab. (LBNL), Berkeley, CA (United States). AmeriFlux; Instituto Tecnologico de Sonora. doi: 10.17190/AMF/1832156

Supporting Information for "Different model assumptions about plant hydraulics and photosynthetic temperature acclimation yield diverging implications for tropical forest resilience"

Claire M. Zarakas[1], Abigail L. S. Swann[1,2], Charles Koven[3], Marielle N. Smith[4,5], and Tyeen C. Taylor[6]

[1]Department of Atmospheric Sciences, University of Washington, Seattle, WA, USA
[2]Department of Biology, University of Washington, Seattle, WA, USA
[3]Lawrence Berkeley National Laboratory, Berkeley, CA, USA
[4]Department of Forestry, Michigan State University, East Lansing, MI, USA
[5]School of Environmental and Natural Sciences, College of Environmental Sciences and Engineering, Bangor University, Bangor, UK
[6]University of Michigan, Department of Civil and Environmental Engineering, Ann Arbor, Michigan, USA

Corresponding author: Claire M. Zarakas, `czarakas@uw.edu`

Text S1 Decomposition of Meteorological Drivers

We decompose the modeled light-saturated GPP into four different components: (1) the direct temperature effect, (2) the VPD effect, (3) the synergistic effect, and (4) other meteorological effects. We first decompose the modeled GPP into the temperature and VPD combined effects and into other meteorological effects, such that $\beta_{total} = \beta_{T+VPD} + \beta_{other}$:

$$\beta_{total} = \Delta GPP_{historical} \tag{1}$$

$$\beta_{T+VPD} = \Delta GPP_{historical} - \Delta GPP_{LowVPDLowTemp} \tag{2}$$

$$\beta_{other} = \Delta GPP_{LowVPDLowTemp} \tag{3}$$

Where ΔGPP_X is the difference between the light-saturated GPP in model experiment X (as described in Table 2) and the historical light-saturated GPP at 25°C. We then further decompose β_{T+VPD} into the direct temperature effect β_T, the VPD effect β_{VPD}, and the synergistic temperature-VPD effect β_{syn}, such that $\beta_{T+VPD} = \beta_T + \beta_{VPD} + \beta_{syn}$:

$$\beta_T = \Delta GPP_{historical} - \Delta GPP_{LowTemp} \tag{4}$$

$$\beta_{VPD} = \Delta GPP_{historical} - \Delta GPP_{LowVPD} \tag{5}$$

$$\beta_{syn} = \beta_{T+VPD} - \beta_T - \beta_{VPD} \tag{6}$$

It follows from these definitions that $\beta_{total} = \beta_T + \beta_{VPD} + \beta_{syn} + \beta_{other}$.

CMIP6 Earth system model	Land Model	Includes Plant Hydraulics?	Includes Photosynthetic Temperature Acclimation?	Plant Hydraulics Implementation	Photosynthetic Temperature Acclimation Implementation
CESM2	CLM5.0	Yes	Yes	Kennedy et al. (2019)	Lombardozzi et al. (2015)[1]
NorESM2-LM	CLM5.0	Yes	Yes	Kennedy et al. (2019)	Lombardozzi et al. (2015)[1]
GFDL-ESM4	GFDL-LM4.1	Yes	No*	Wolf et al. (2016)	Smith et al. (2016)
IPSL-CM6A-LR	ORCHIDEE (v2.0, Water/Carbon/Energy)	No*	Yes	Naudts et al. (2015), Yao et al. (2022)	Vuichard et al. (2019)[1]
CMCC-ESM2	CLM4.5 (BGC mode)	No	Yes	NA	
BCC-CSM2-MR	BCC_AVIM2	No	Yes	NA	
ACCESS-ESM1-5	CABLE2.4	No*	No*	De Kauwe et al. (2020, 2022)	Knauer et al. (2023)[2]
UKESM1-0-LL	JULES-ES-1.0	No*	No*	Eller et al. (2018, 2020)	Mercado et al. (2018)[1], Oliver et al. (2022)[1]
GISS-E2-1-G	GISS LSM	No*	No		NA
E3SM-1-1	ELM (v1.1)	No*	No		NA
EC-Earth-CC	HTESSEL and LPJ-GUESS v4	No*	No	Hickler et al. (2006)	NA
MPI-ESM1-2-LR	JSBACH3.20	No	No*	NA	Goll (2013)[1]
MIROC-ES2L	MATSIRO6.0+VISIT-e ver.1.0	No	No	NA	NA
CanESM5	CLASS3.6/CTEM1.2	No	No	NA	NA
CNRM-ESM2-1	Surfex 8.0c	No	No	NA	NA
MRI-ESM2-0	HAL 1.0	No	No	NA	NA

* There are versions of the land model that include this process (e.g. for specific scientific projects) or model implementation of this process is currently being developed, but these processes are not active in the land model codebase that was used in CMIP6 coupled Earth system model simulations.
[1] These models implement the Kattge and Knorr (2007) temperature acclimation scheme
[2] These models implement the Kumarathunge et al.(2019) temperature acclimation scheme

Table S1: Processes included in CMIP6 land models. The table includes all Earth system models participating in the Coupled Climate–Carbon Cycle Model Intercomparison Project (C4MIP; Jones et al., 2016).

Experiment Name	Meteorological Forcing (at the lowest atmospheric level)						
	Temperature	Relative Humidity (%)	Incident solar radiation	Precipitation	Incident longwave radiation	Wind	Surface pressure
Historical	Historical	Historical	Historical	Historical	Historical	Historical	Historical
LowVPD	Historical	Modified so that VPD is 0.4 kPa*	Historical	Historical	Historical	Historical	Historical
LowTemp	25°C	Modified so that the VPD matches the historical VPD	Historical	Historical	Historical	Historical	Historical
LowVPDLowTemp	25°C	Modified so that VPD is 0.4 kPa*	Historical	Historical	Historical	Historical	Historical

* Modified so that VPD at the lowest atmosphere level is 0.4 kPa, which is the average VPD at temperatures 24.5-25.5°C in the historical record.

Table S2: Description of synthetic meteorological forcings.

FATES parameter	FATES parameter description	Default Value	Low Perturbation	Median Perturbation	High Perturbation	Reference for parameter ranges
fates_hydr_kmax_node	maximum xylem conductivity per unit conducting xylem area [kg/MPa/m/s]	3	0.105	3.43	16.038	Christofferson et al. (2021)
fates_leaf_stomatal_slope_ballberry	stomatal slope parameter for Ball-Berry model [unitless]	8	6.98	10.62	18.07	Lin et al. (2015)
fates_hydr_p50_node*	xylem water potential at 50% loss of conductivity	-2.25	-6.3	-1.79	-0.18	Christofferson et al. (2021)
fates_leaf_vcmax25top	maximum carboxylation rate of Rub. at 25C, canopy top	60	7.78	45	60.1	Albert et al. (2018)

Table S3: Parameter perturbations included in the small perturbed parameter ensemble. For each parameter (each row), three one-at-a-time parameter perturbation experiments were simulated: one low-end simulation, one median, and one high-end simulation, where the low-end, median, and high-end parameter perturbation values were determined based on literature review.

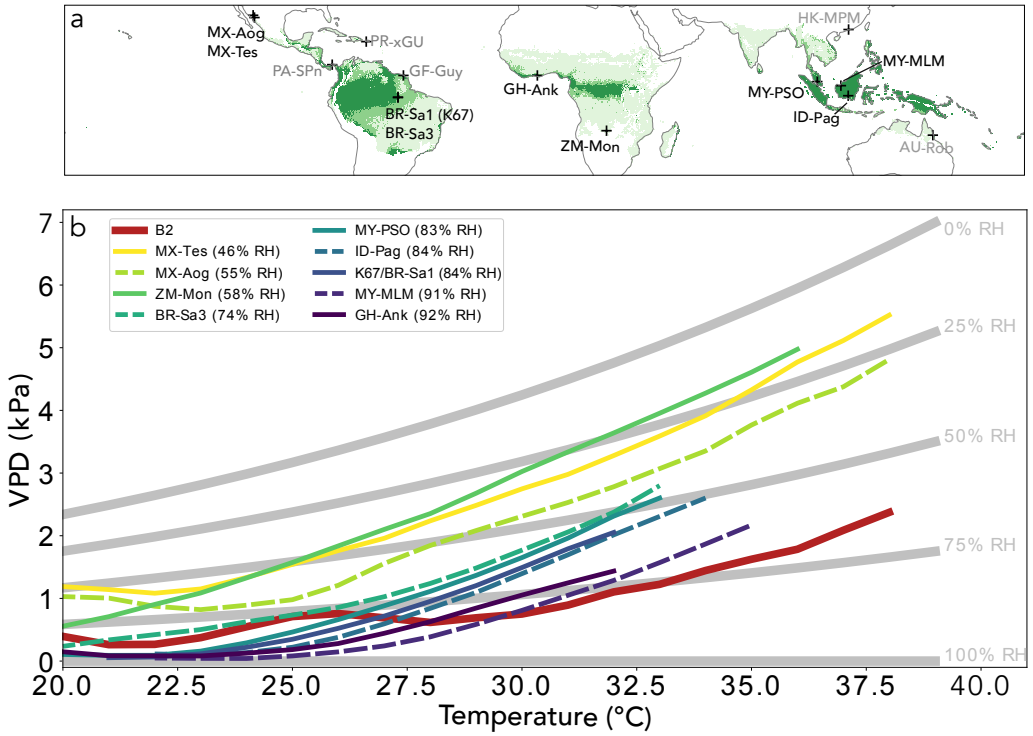

Figure S1: Temperature-VPD regimes of study sites, compared to other tropical forest sites. (a) Location of tropical forest sites used in this study, along with other tropical forest sites in the FLUXNET and/or Ameriflux networks which have a mean annual temperature > 20°C and are classified as deciduous or evergreen broadleaf tropical forests. Colors indicate the extent of tropical Köppen-Geiger climate classifications (Köppen, 1936; Peel et al., 2007) as calculated from ERA5 Reanalysis (European Centre for Medium-Range Weather Forecasts, 2019). (b) Temperature-VPD relationships for tropical forest sites, based on FLUXNET and/or Ameriflux meteorological data. Curves are calculated by binning VPD by air temperature in 1°C bins, and calculating the mean VPD for each temperature bin. Lines are colored to indicate natural forest sites' average relative humidity. Gray background curves indicate the temperature-VPD relationship for a given relative humidity level.

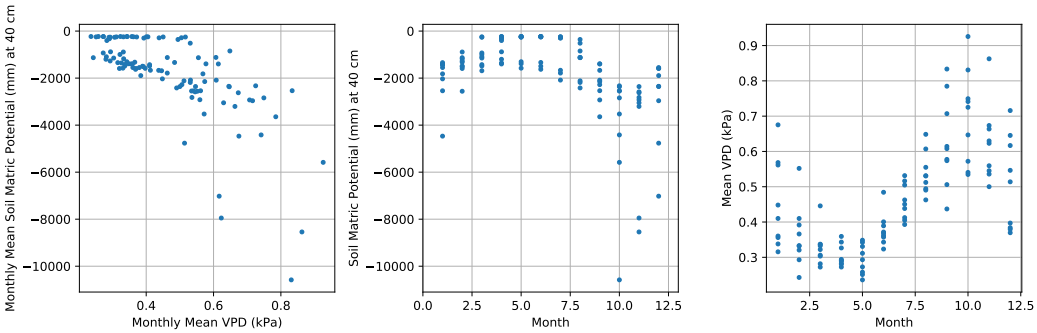

Figure S2: Variation in VPD and soil moisture on monthly timescales. (a) Relationship between monthly mean VPD at 2m and monthly mean soil matric potential (SMP) at 40 cm depth (note that more negative SMP corresponds to drier soils). Seasonal cycles of (b) SMP and (c) VPD.

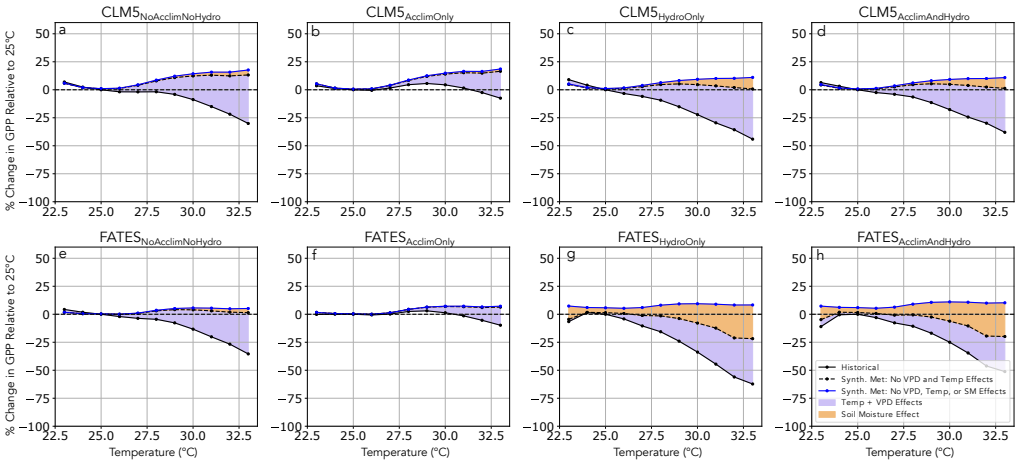

Figure S3: Soil moisture influences on the apparent GPP response to temperature at K67 for different configurations of CLM5 (a-d) and FATES (e-h). Shaded areas show how much the modeled apparent GPP response to temperature (black line) are due to the combination of temperature and VPD effects (purple shaded area) and soil moisture effects (orange area). These meteorological effects are calculated from synthetic meteorology simulations where temperature and VPD are held constant (dashed black line) and where precipitation is held constant at 0.005 mm/s to fully saturate the soil at all points in time (blue line).

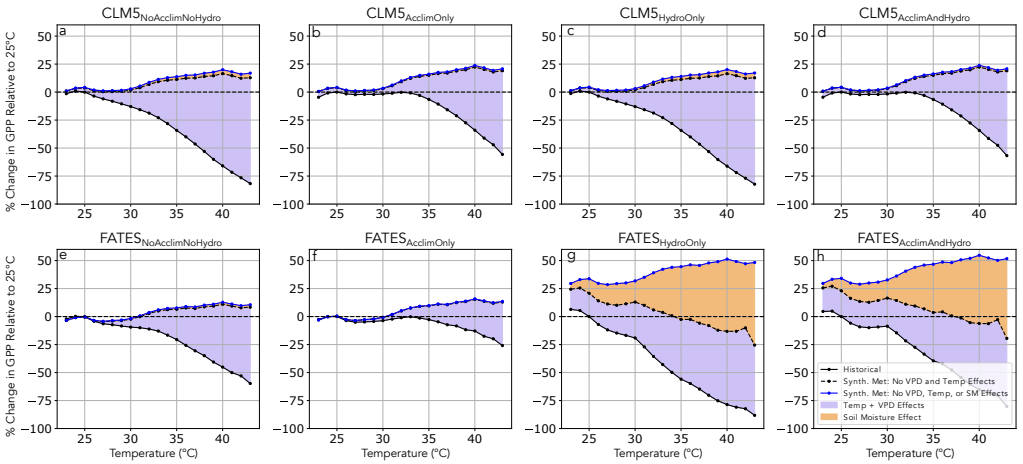

Figure S4: Soil moisture influences on the apparent GPP response to temperature at Biosphere 2. As in Figure 3, but at Biosphere 2.

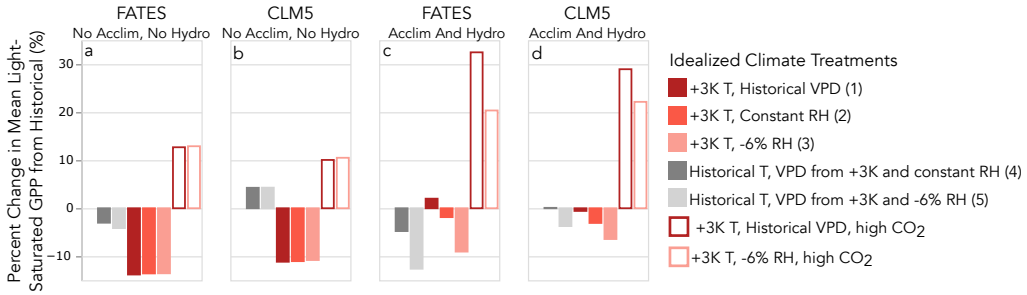

Figure S5: Mean light-saturated GPP responses at K67 to idealized climate treatments for different model configurations: (a) FATES without temperature acclimation or plant hydraulics, (b) CLM5 without temperature acclimation or plant hydraulics, (c) FATES with active temperature acclimation and plant hydraulics, and (d) CLM5 with active temperature acclimation and plant hydraulics. Solid bars indicate the mean GPP change when the atmospheric CO_2 concentration is held constant at historical levels, and empty bars indicate the change when atmospheric CO_2 concentration is elevated to 560 ppm.

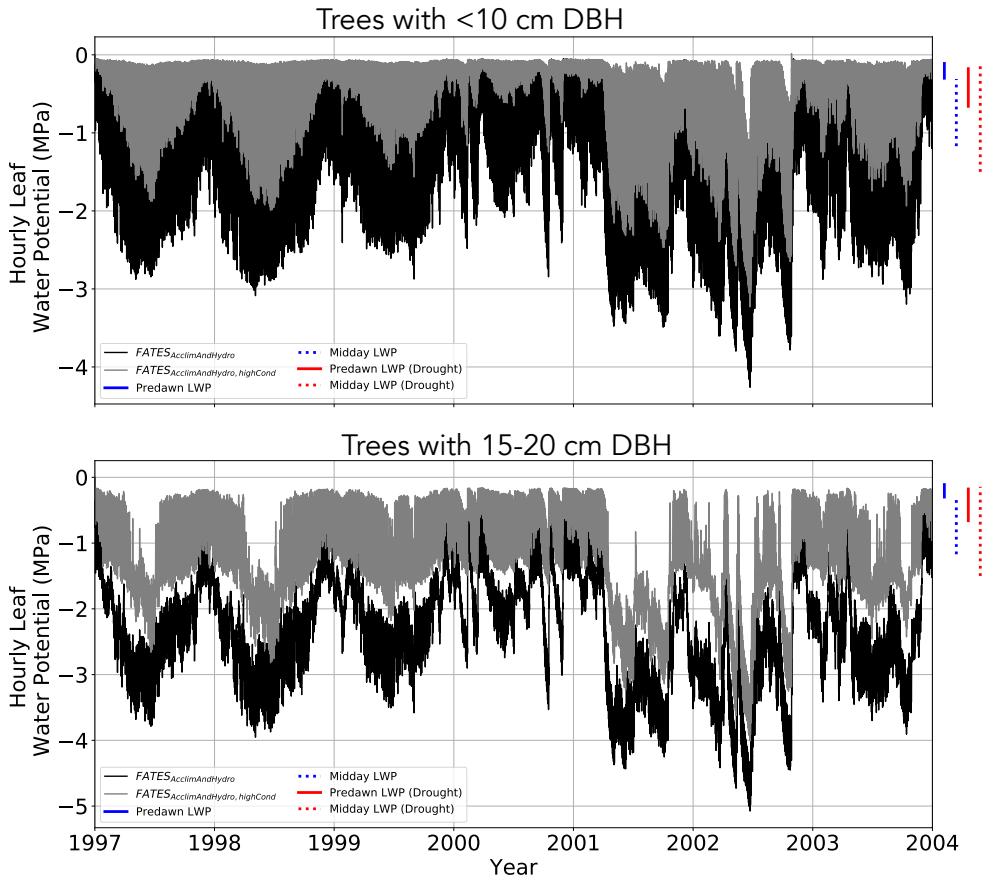

Figure S6: Modeled leaf water potential for FATES$_{\text{AcclimAndHydro}}$, with default parameters (black) compared to increased maximum hydraulic conductivity (gray). Bars to the right of the plots indicate the range of leaf water potential observations collected in 2002 at Biosphere 2 (Pegoraro et al., 2006) in normal conditions (blue) and during a drought experiment (red).

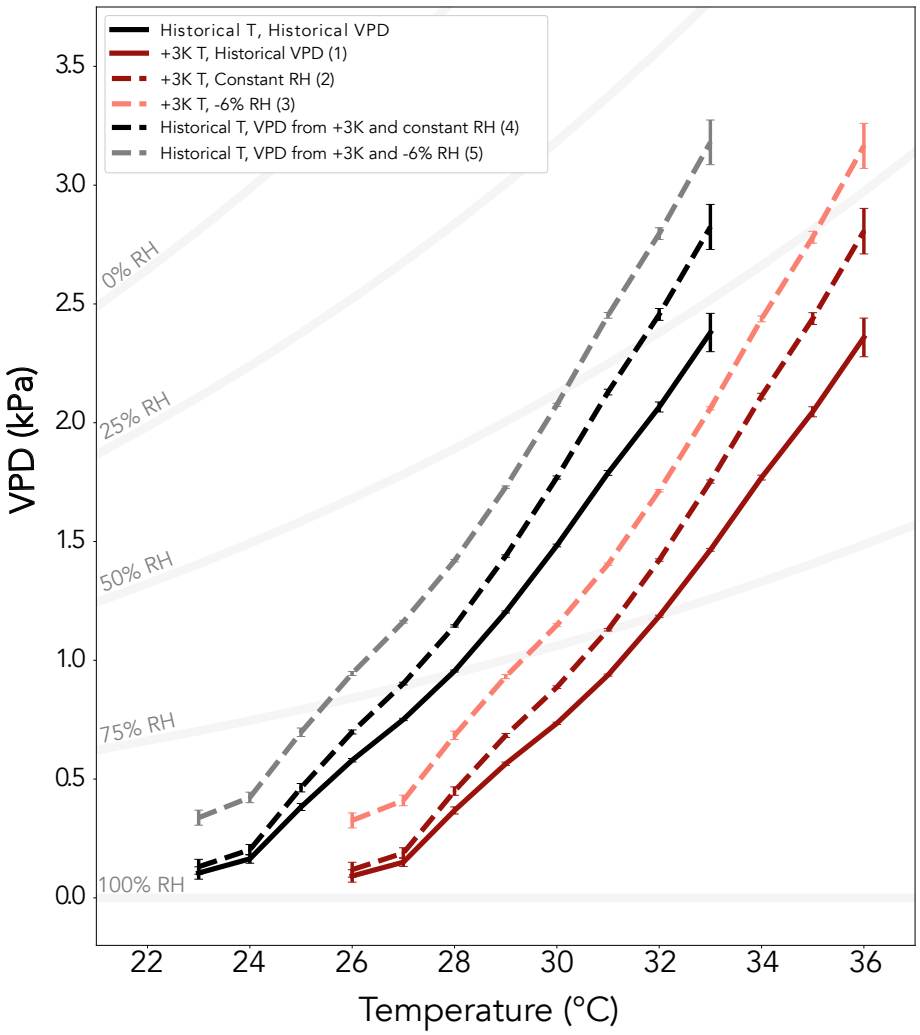

Figure S7: Idealized climate treatments in temperature-VPD space. Gray background curves indicate the temperature-VPD relationship for a given relative humidity level. Numbers in the legend correspond to the idealized climate treatment numbers in the main text.

References

Albert, L. P., Wu, J., Prohaska, N., de Camargo, P. B., Huxman, T. E., Tribuzy, E. S., ... Saleska, S. R. (2018). Age-dependent leaf physiology and consequences for crown-scale carbon uptake during the dry season in an Amazon evergreen forest. *New Phytologist*, *219*(3), 870–884. doi: 10.1111/nph.15056

Christoffersen, B. O. (2021). Pantropical tropical tree xylem hydraulic functional traits, 1991 - 2013. 1.0. NGEE Tropics Data Collection. doi: http://dx.doi.org/10.15486/ngt/1581482

Christoffersen, B. O., Gloor, M., Fauset, S., Fyllas, N. M., Galbraith, D. R., Baker, T. R., ... Meir, P. (2016, November). Linking hydraulic traits to tropical forest function in a size-structured and trait-driven model (TFS v.1-Hydro). *Geoscientific Model Development*, *9*(11), 4227–4255. doi: 10.5194/gmd-9-4227-2016

De Kauwe, M. G., Medlyn, B. E., Ukkola, A. M., Mu, M., Sabot, M. E. B., Pitman, A. J., ... Briggs, P. R. (2020). Identifying areas at risk of drought-induced tree mortality across South-Eastern Australia. *Global Change Biology*, *26*(10), 5716–5733. doi: 10.1111/gcb.15215

De Kauwe, M. G., Sabot, M. E. B., Medlyn, B. E., Pitman, A. J., Meir, P., Cernusak, L. A., ... Choat, B. (2022). Towards species-level forecasts of drought-induced tree mortality risk. *New Phytologist*, *235*(1), 94–110. doi: 10.1111/nph.18129

Eller, C. B., de V. Barros, F., Bittencourt, P. R., Rowland, L., Mencuccini, M., & Oliveira, R. S. (2018). Xylem hydraulic safety and construction costs determine tropical tree growth. *Plant, Cell & Environment*, *41*(3), 548–562. doi: 10.1111/pce.13106

Eller, C. B., Rowland, L., Mencuccini, M., Rosas, T., Williams, K., Harper, A., ... Cox, P. M. (2020). Stomatal optimization based on xylem hydraulics (SOX) improves land surface model simulation of vegetation responses to climate. *New Phytologist*, *226*(6), 1622–1637. doi: 10.1111/nph.16419

European Centre for Medium-Range Weather Forecasts. (2019). *ERA5 Reanalysis (Monthly Mean 0.25 Degree Latitude-Longitude Grid).* Research Data Archive at the National Center for Atmospheric Research, Computational and Information Systems Laboratory.

Goll, D. (2013). *The influence of phosphorus cycling and temperature acclimation of photosynthesis on the land carbon cycle* (Doctoral dissertation, Hamburg University Hamburg). doi: 10.17617/2.1669156

Hickler, T., Prentice, I. C., Smith, B., Sykes, M. T., & Zaehle, S. (2006). Implementing plant hydraulic architecture within the LPJ Dynamic Global Vegetation Model. *Global Ecology and Biogeography*, *15*(6), 567–577. doi: 10.1111/j.1466-8238.2006.00254.x

Jones, C. D., Arora, V., Friedlingstein, P., Bopp, L., Brovkin, V., Dunne, J., ... Zaehle, S. (2016, August). C4MIP – The Coupled Climate–Carbon Cycle Model Intercomparison Project:experimental protocol for CMIP6. *Geoscientific Model Development*, *9*(8), 2853–2880. doi: 10.5194/gmd-9-2853-2016

Kattge, J., & Knorr, W. (2007). Temperature acclimation in a biochemical model of photosynthesis: a reanalysis of data from 36 species. *Plant, Cell & Environment*, *30*(9), 1176–1190. doi: 10.1111/j.1365-3040.2007.01690.x

Kennedy, D., Swenson, S., Oleson, K. W., Lawrence, D. M., Fisher, R., Costa, A. C. L. d., & Gentine, P. (2019). Implementing Plant Hydraulics in the Community Land Model, Version 5. *Journal of Advances in Modeling Earth Systems*, *11*(2), 485–513. doi: https://doi.org/10.1029/2018MS001500

Knauer, J., Cuntz, M., Smith, B., Canadell, J. G., Medlyn, B. E., Bennett, A. C., ... Haverd, V. (2023, November). Higher global gross primary productivity under future climate with more advanced representations of photosynthesis. *Science Advances*, *9*(46), eadh9444. doi: 10.1126/sciadv.adh9444

Kumarathunge, D. P., Medlyn, B. E., Drake, J. E., Tjoelker, M. G., Aspinwall, M. J., Battaglia, M., ... Way, D. A. (2019). Acclimation and adaptation components of the temperature dependence of plant photosynthesis at the global scale. *New Phytologist*, *222*(2), 768–784. doi: https://doi.org/10.1111/nph.15668

Köppen, W. (1936). Das Geographische System der Klimate. In *Handbuch der klimatologie.*

Lin, Y.-S., Medlyn, B. E., Duursma, R. A., Prentice, I. C., Wang, H., Baig, S., ... Wingate, L. (2015, May). Optimal stomatal behaviour around the world. *Nature Climate Change*, *5*(5), 459–464. doi: 10.1038/nclimate2550

Lombardozzi, D. L., Bonan, G. B., Smith, N. G., Dukes, J. S., & Fisher, R. A. (2015). Temperature acclimation of photosynthesis and respiration: A key uncertainty in the carbon cycle-climate feedback. *Geophysical Research Letters*, *42*(20), 8624–8631. doi: https://doi.org/10.1002/2015GL065934

Mercado, L. M., Medlyn, B. E., Huntingford, C., Oliver, R. J., Clark, D. B., Sitch, S., ... Cox, P. M. (2018). Large sensitivity in land carbon storage due to geographical and temporal variation in the thermal response of photosynthetic capacity. *New Phytologist*, *218*(4), 1462–1477. doi: 10.1111/nph.15100

Naudts, K., Ryder, J., McGrath, M. J., Otto, J., Chen, Y., Valade, A., ... Luyssaert, S. (2015, July). A vertically discretised canopy description for ORCHIDEE (SVN r2290) and the modifications to the energy, water and carbon fluxes. *Geoscientific Model Development*, *8*(7), 2035–2065. doi: 10.5194/gmd-8-2035-2015

Oliver, R. J., Mercado, L. M., Clark, D. B., Huntingford, C., Taylor, C. M., Vidale, P. L., ... Medlyn, B. E. (2022, July). Improved representation of plant physiology in the JULES-vn5.6 land surface model: photosynthesis, stomatal conductance and thermal acclimation. *Geoscientific Model Development*, *15*(14), 5567–5592. doi: 10.5194/gmd-15-5567-2022

Peel, M. C., Finlayson, B. L., & McMahon, T. A. (2007, October). Updated world map of the Köppen-Geiger climate classification. *Hydrology and Earth System Sciences*, *11*(5), 1633–1644. doi: 10.5194/hess-11-1633-2007

Pegoraro, E., Rey, A., Abrell, L., Haren, J. V., & Lin, G. (2006). Drought effect on isoprene production and consumption in Biosphere 2 tropical rainforest. *Global Change Biology*, *12*(3), 456–469. doi: https://doi.org/10.1111/j.1365-2486.2006.01112.x

Smith, N. G., Malyshev, S. L., Shevliakova, E., Kattge, J., & Dukes, J. S. (2016, April). Foliar temperature acclimation reduces simulated carbon sensitivity to climate. *Nature Climate Change*, *6*(4), 407–411. doi: 10.1038/nclimate2878

Wolf, A., Anderegg, W. R. L., & Pacala, S. W. (2016, November). Optimal stomatal behavior with competition for water and risk of hydraulic impairment. *Proceedings of the National Academy of Sciences*, *113*(46), E7222–E7230. doi: 10.1073/pnas.1615144113

Yao, Y., Joetzjer, E., Ciais, P., Viovy, N., Cresto Aleina, F., Chave, J., ... Luyssaert, S. (2022, October). Forest fluxes and mortality response to drought: model description (ORCHIDEE-CAN-NHA r7236) and evaluation at the Caxiuanã drought experiment. *Geoscientific Model Development*, *15*(20), 7809–7833. doi: 10.5194/gmd-15-7809-2022